Research Paper

THEMED ISSUE: Mantle to Surface Dynamics during the Transition from Subduction to Collision to Tectonic Escape: Results from the Continental Dynamics–Central Anatolian Tectonics (CD-CAT) Project

GEOSPHERE

GEOSPHERE, v. 16

https://doi.org/10.1130/GES02175.1

6 figures; 1 supplemental file

CORRESPONDENCE: lindsay.schoenbohm@utoronto.ca

CITATION: Krystopowicz, N.J., Schoenbohm, L.M., Rimando, J., Brocard, G., and Rojay, B., 2020, Tectonic geomorphology and Plio-Quaternary structural evolution of the Tuzgölü fault zone, Turkey: Implications for deformation in the interior of the Central Anatolian Plateau: Geosphere, v. 16, https://doi.org/10.1130/GES02175.1.

Science Editor: Andrea Hampel
Guest Associate Editor: Paul Umhoefer

Received 5 July 2019
Revision received 8 May 2020
Accepted 25 June 2020

GOLD OPEN ACCESS

THE GEOLOGICAL SOCIETY OF AMERICA®

This paper is published under the terms of the CC-BY-NC license.

© 2020 The Authors

Tectonic geomorphology and Plio-Quaternary structural evolution of the Tuzgölü fault zone, Turkey: Implications for deformation in the interior of the Central Anatolian Plateau

Neil J. Krystopowicz[1], Lindsay M. Schoenbohm[1,2], Jeremy Rimando[1], Gilles Brocard[3], and Bora Rojay[4]

[1]Department of Earth Sciences, University of Toronto, Toronto, Ontario M5S 3B1, Canada
[2]Department of Chemical and Physical Sciences, University of Toronto Mississauga, Mississauga, Ontario L5L 1C6, Canada
[3]Archéorient, Maison de l'Orient et de La Méditerranée, 7 Rue Raulin, 69007 Lyon, Université de Lyon 2, France
[4]Department of Geological Engineering, Middle East Technical University, 06531 Ankara, Turkey

ABSTRACT

Situated within the interior of the Central Anatolian Plateau (Turkey), the 200-km-long Tuzgölü extensional fault zone offers first-order constraints on the timing and pattern of regional deformation and uplift. In this study, we analyze the morphometrics of catchments along the Tuzgölü range-front fault and the parallel, basinward Hamzalı fault using a variety of measured morphometric indicators coupled with regional geomorphic observations and longitudinal profile analysis. In addition, we use field and remote mapping to constrain the geometry of two key marker beds, the Pliocene Kızılkaya ignimbrite and Kışladağ limestone, in order to investigate deformation in the footwall of the Tuzgölü fault zone. The marker beds form a broad arch along the footwall of the fault, with greatest cumulative displacement along the central part of the fault zone, suggesting early Pliocene extensional reactivation of the Tuzgölü fault with a typical fault-displacement profile. However, a change in deformation pattern is marked by transient knickpoints along river channels; morphometric indicators sensitive to shorter (1–3 Ma) time scales, including river steepness, basin elongation, and mountain front sinuosity, indicate an overall southeastward increase in footwall uplift rate of the Tuzgölü fault zone, which could reflect block rotation or interaction with the Hasan Dag volcano. Basin asymmetry and basin-fault azimuth measurements indicate north-northwest tilting of footwall catchments, which may be linked to regional tilting across the Central Anatolian Plateau interior. Varying patterns of spatial and temporal deformation along the length of the Tuzgölü fault zone are likely due to the interference of crustal- and lithospheric-scale processes, such as rotation of crustal blocks, extrusion of the Anatolian microplate, crustal heating, gravitational collapse associated with plateau uplift, and mantle-driven vertical displacements.

INTRODUCTION

The Central Anatolian Plateau (Turkey; Fig. 1A), as with other plateaus around the world, is a product of competing (or complementary) tectonic, geodynamic, kinematic, and magmatic forces. For example, crustal shortening and thickening, lithospheric mantle delamination, lower-crustal flow, and dynamic topography have all been invoked to explain broad, regionally uplifted areas such as the Central Andes (Kay and Mahlburg Kay, 1993; Kay et al., 1994; Yuan et al., 2002), Sierra Nevada (Jones et al., 2004; Zandt et al., 2004), Tibet (Clark et al., 2005; Wang et al., 2008), and Anatolia (Faccenna and Becker, 2010; Bartol and Govers, 2014; Fernández-Blanco, 2014; Göğüş et al., 2017; Meijers et al., 2018; D. Fernández-Blanco, personal commun., 2019). Slab breakoff, magmatic underplating, and changes in slab dip may also induce deformation and uplift in the overriding plate (Jordan et al., 1983; Brown, 1994; Davies and von Blanckenburg, 1995; Gutscher et al., 2000; Duretz et al., 2011; Abgarmi et al., 2017; Delph et al., 2017). As regional deformation progresses, the rotation of continental blocks produces variable strain along fault segments (e.g., Jackson and Molnar, 1990; Westaway, 1990; Price and Scott, 1994). Finally, faults may interact with regional magmatism, with the location and morphology of volcanoes reflecting fault geometry (Dhont et al., 1998; Toprak, 1998; Paulsen and Wilson, 2010), or slip rates reflecting intrusion of magma (Bull et al., 2003; Villamor et al., 2007; Mathieu et al., 2011).

In this study, we seek to understand potential drivers of deformation in Anatolia and how they interact and evolve over time. To do this, we constrain the timing and pattern of deformation along the Tuzgölü fault system, which is situated within the interior of the Central Anatolian Plateau along the eastern margin of the Tuzgölü Basin. It consists of the 200-km-long, northwest-striking Tuzgölü fault and the parallel, 20-km-long, basinward Hamzalı fault. The fault system first formed as early as the late Maastrichtian (Görür and Derman, 1978; Görür et al., 1984; Çemen et al., 1999; Derman et al., 2003; Özsayin et al., 2013), was reactivated as a strike-slip fault in the Eocene (Çemen et al., 1999; Robertson et al., 2009), and experienced compression in the late Miocene to early Pliocene (Fernández-Blanco et al., 2013). It is currently dominated by extension, with a possible right-slip component (Çemen et al., 1999; Derman et al., 2003; Koçyiğit and Özacar, 2003; Özsayin et al., 2013). The southern end of the Tuzgölü fault crosses and interacts with the Central Anatolian volcanic province (Toprak, 1998; Schlieffarth et al., 2019), slicing through the northeastern edge of the Hasan Dag volcano (Dhont et al., 1998). Paleoseismic trenching

Lindsay M. Schoenbohm https://orcid.org/0000-0001-7898-356X

Downloaded from https://pubs.geoscienceworld.org/gsa/geosphere/article-pdf/doi/10.1130/GES02175.1/5097193/ges02175.pdf
by guest

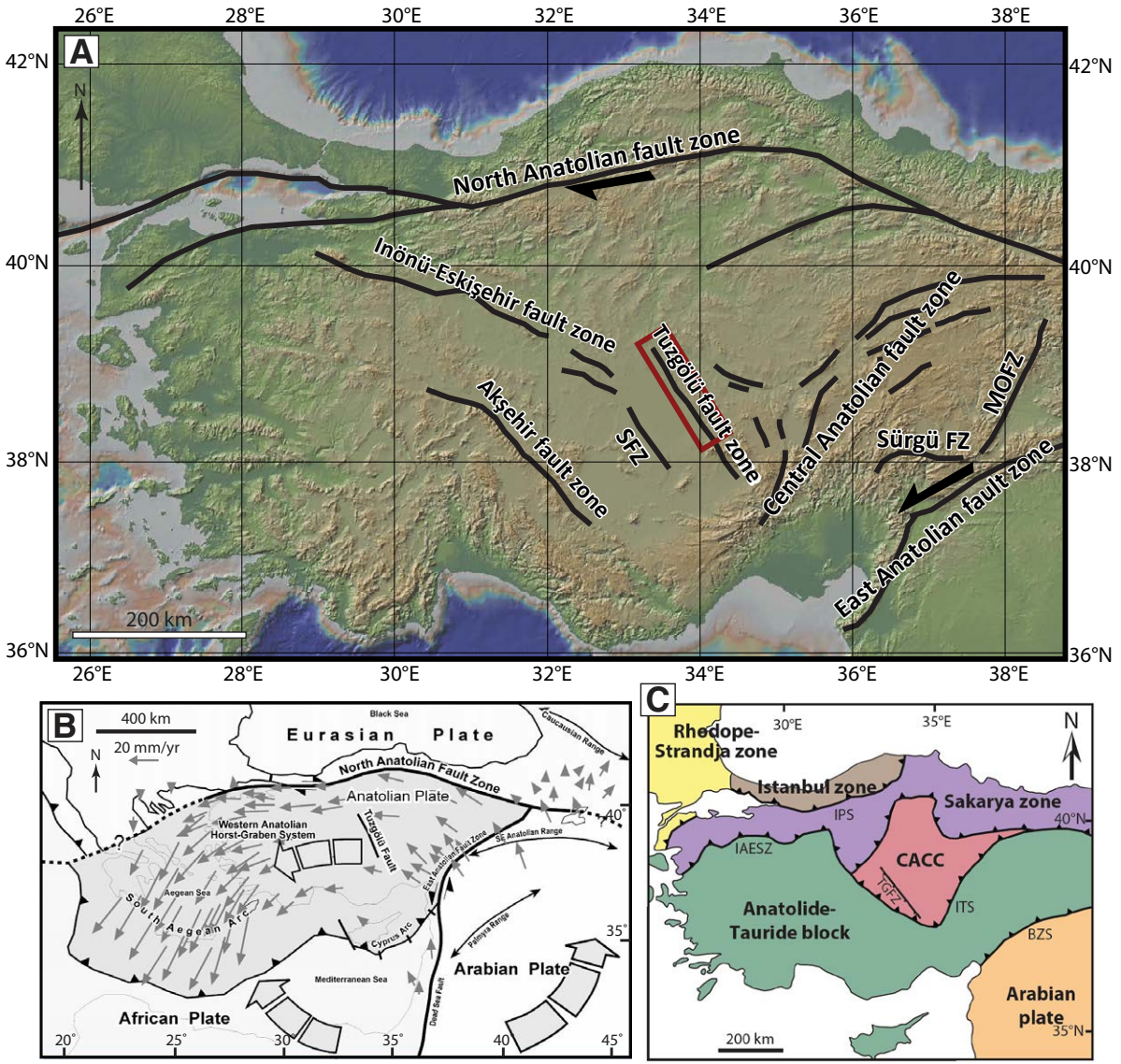

Figure 1. Regional morphology, structures, tectonics, and terranes of Central Anatolia, Turkey. (A) Regional faults on a Shuttle Radar Topography Mission (SRTM)–based digital elevation model (90 m). FZ—fault zone; MOFZ—Malatya-Ovacık fault zone; SFZ—Sultanhanı fault zone. Red box marks approximate locations of Figures 2, 3, 5, and 6. (B) Simplified tectonic map of the eastern Mediterranean region showing GPS-determined horizontal velocities with thin, gray arrows in a Eurasian-fixed reference frame (modified from McClusky et al., 2000). Thick, segmented arrows show generalized motion of plates. (C) Regional map showing major tectonic boundaries and sutures. CACC—Central Anatolian Crystalline Complex; IPS—Intra-Pontide suture; IAESZ—Izmir-Ankara-Erzincan suture zone; ITS—Inner Tauride suture; BZS—Bitlis-Zagros suture; TGFZ—Tuzgölü fault zone.

Downloaded from https://pubs.geoscienceworld.org/gsa/geosphere/article-pdf/doi/10.1130/GES02175.1/5097193/ges02175.pdf
by guest

indicates that the Tuzgölü fault is seismically active, with evidence for past events as large as M_w 6.7 (Kürçer and Gökten, 2012), thus posing a significant danger for the region.

Because of the rapid evolution of the Tuzgölü fault zone in the face of complex regional deformation, a full understanding of deformation along this and other regional faults requires techniques that are sensitive to different temporal and spatial scales. In this study, we capture Pliocene deformation of the footwall of the Tuzgölü fault by measuring deflection of two key Pliocene-aged marker beds. To address deformation in the last few million years, we analyze the shape of uplifted rivers in profile (e.g., Wobus et al., 2006) in 23 major catchments in the footwall of the Tuzgölü fault. Finally, to understand the most recent (<~1 Ma) and most spatially restricted phase of deformation, we measure geomorphic parameters in 92 small (<10 km^2) catchments immediately adjacent to the Tuzgölü and Hamzalı faults, including catchment hypsometry, elongation, asymmetry, and orientation (Strahler, 1952; Schumm, 1956; Hare and Gardner, 1985), and the sinuosity of the mountain front (Bull and McFadden, 1977). A combination of techniques sensitive to different temporal and spatial scales can best reveal links between deformation and geodynamic drivers. We use our results to understand the relationship between the Tuzgölü fault zone and regional tectonic deformation, and further our understanding of the connection between landscape evolution and the mechanisms responsible for generating high topography, volcanism, extension, and block rotation in Central Anatolia.

REGIONAL SETTING

Studies using GPS show that the westward motion of the Anatolian plate relative to Eurasia (Reilinger et al., 1997; McClusky et al., 2000; Reilinger et al., 2006) is accommodated along two first-order structures: the dextral North Anatolian fault zone and the sinistral East Anatolian fault zone (Ketin, 1948; McKenzie, 1976; Şengör and Kidd, 1979; Dewey and Şengör, 1979; Şengör et al., 1985). One driving force behind this westward translation may be gravitational pull from slab rollback associated with subduction at the Hellenic trench, producing extensional deformation in the overriding Anatolian microplate (Le Pichon, 1982; Reilinger et al., 2006; Jolivet et al., 2013). However, westward translation may also partly result from lateral extrusion away from the Arabia-Eurasia collision zone (McKenzie, 1972; Dewey and Şengör, 1979; Dewey et al., 1986). As westward translation occurs, the Anatolian microplate undergoes internal deformation accommodated by transtensional and transpressional strain and strike-slip displacement (Şengör et al., 1985; Umhoefer et al., 2007; Genç and Yürür, 2010; Özsayin and Dirik, 2011).

The northern and southern margins of the Central Anatolian Plateau consist of the Pontide and Tauride orogenic belts, respectively. These formed during Paleogene to Miocene closure of the Izmir-Ankara-Erzincan and Inner Tauride oceans through collision between the Anatolide-Tauride, Sakarya, and Central Anatolian Crystalline Complex belts (Fig. 1C) (e.g., Şengör and Yılmaz, 1981; Şengör et al., 1985; Robertson et al., 1996; Yılmaz et al., 1997; Robertson et al., 2009). Uplift along the northern margin of the plateau may be related to late Miocene to late Pleistocene strain accumulation across a broad restraining bend in the North Anatolian fault zone (Yildirim et al., 2011). The southern Central Anatolian Plateau margin has experienced ~2 km of rapid uplift of marine sediments in the Central Taurides since the late Miocene (e.g., Cosentino et al., 2012; Schildgen et al., 2012a, 2012b; Meijers et al., 2018), with an acceleration after 1.6 Ma (Schildgen et al., 2012a). Shortening of the Central Taurides could be the source of at least some of this uplift (Walsh-Kennedy et al., 2014; Fernández-Blanco et al., 2018), as could rollback of the Cyprus slab and slab fragmentation, breakoff, or necking (Delph et al., 2017; Abgarmi et al., 2017). The acceleration of uplift rate after 1.6 Ma could have been caused by complete slab detachment (Delph et al., 2017) and/or by entry of the Eratosthenes seamount into the Cyprus trench (Schildgen et al., 2012a, 2014).

The timing of uplift of the interior of the Central Anatolian Plateau, where the Tuzgölü fault zone is located, is poorly constrained. Presently, the plateau interior is characterized by relatively low relief (<500 m) and elevations (~1 km), compared to its elevated (~2 km), high-relief margins. Sedimentological, paleoaltimetric, and paleoclimatic studies suggest that much of the Tuzgölü region, particularly the southern Tuzgölü Basin, switched to a terrestrial setting in the middle Miocene (e.g., Dercourt et al., 1993; Popov et al., 2004, 2006; Akgün et al., 2007; Ćorić et al., 2012; Aydar et al., 2013; Landau et al., 2013), implying onset of uplift by that time. Stable oxygen isotope data from lacustrine carbonates within the plateau interior suggest uplift between ca. 11 and 5 Ma, with elevations similar to present reached by 5 Ma (Meijers et al., 2018). Uplift may have been caused by Miocene slab retreat and delamination of mantle lithosphere (Bartol and Govers, 2014), oroclinal bending and resulting foundering of the mantle lithosphere (Göğüş et al., 2017), or dynamic upwelling of asthenospheric mantle (Faccenna and Becker, 2010).

Although major westward motion of Anatolia is accommodated by dextral displacement along the North Anatolian fault zone to the north and sinistral displacement along the East Anatolian fault zone to the southeast (Figs. 1A and 1B), a number of structures within the Central Anatolian Plateau interior accommodate regional deformation. Sinistral faults that trend generally west-southwest include the Central Anatolian fault zone (Koçyiğit and Beyhan, 1998; Higgins et al., 2015), the Malatya-Ovacık fault zone (Kaymakcı et al., 2006; Westaway et al., 2008), and the Sürgü fault (Koç and Kaymakcı, 2013) (Fig. 1A). West of the Central Anatolian fault zone, the Tuzgölü fault zone strikes northwest and accommodates dextral, normal displacement, bounding the eastern edge of the Tuzgölü Basin. The similarly oriented Sultanhanı fault zone (Melnick et al., 2017) marks the western side of the Tuzgölü Basin. Farther west, the Inönü-Eskişehir and Akşehir fault zones (Özsayın and Dirik, 2011) accommodate extension and dextral strike-slip.

The Tuzgölü fault zone, which includes the Tuzgölü and Hamzalı faults, stretches from the Paşdağ Mountain in the northwest to beyond the Hasan Dag volcano in the southeast (Figs. 1 and 2). We restrict our study to the fault segments adjacent to the Tuzgölü Basin. The fault system consists of 10 major southwest-dipping segments, as well as various minor northeast- and

Downloaded from https://pubs.geoscienceworld.org/gsa/geosphere/article-pdf/doi/10.1130/GES02175.1/5097193/ges02175.pdf
by guest

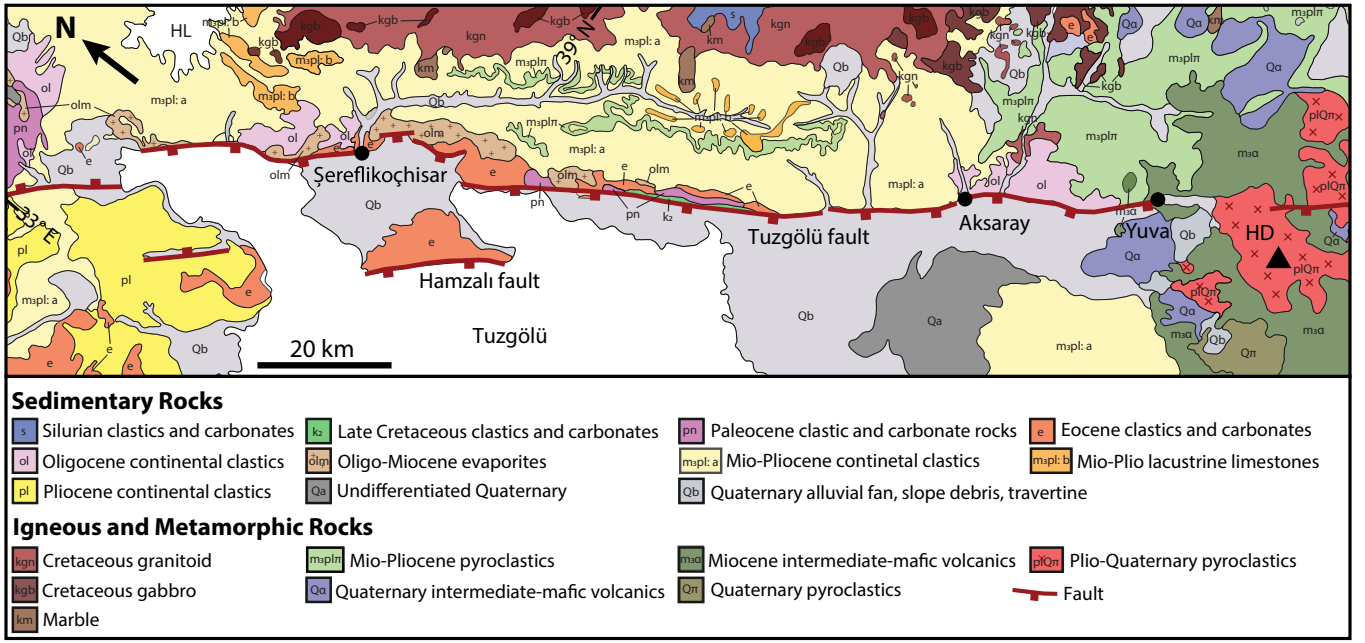

Figure 2. Active faults and geological units along the Tuzgölü fault zone (see Fig. 1 for location). HL—Hırfanlı Lake; HD—Hasan Dag volcano. This map was modified from a 1:250,000-scale geological map of Turkey (Akbaş, 2011) prepared by the Mineral Research and Exploration Institute of Turkey (MTA). Area is similar to that of Figures 5 and 6.

southwest-dipping faults. Based on seismic reflection data, the main fault strand is listric in the subsurface (Çemen et al., 1999). The Hamzalı fault, ~20 km long with the same orientation as the Tuzgölü fault, is located 12 km basinward along the Şereflikoçhisar Peninsula (Fig. 2).

Most of the Tuzgölü footwall displays uniform lithology (Fig. 2; Geological Research Department, 1989a, 1989b), consisting of upper Miocene and Pliocene continental clastics and lacustrine limestones, i.e., the former basin floor exposed by uplift along the fault. Underlying units of Oligocene to lower Miocene gypsum, as well as sandstones, shales, and conglomerates of Eocene and Oligocene age, are exposed near the town of Şereflikoçhisar. Southeast of Aksaray, lithology is dominated by Oligocene continental clastics and volcanic rocks of Plio-Quaternary age. The footwall rocks of the Hamzalı scarp consist of sandstones, shales, and interbedded limestones of Eocene age.

The footwall of the Tuzgölü fault is elevated several hundred meters above the Tuzgölü Basin. A longitudinal river runs northwest, parallel to the trace of the fault, ~10 km into the interior of the footwall (Fig. 3). The divide between the range front and the longitudinal river is offset to the northeast. Catchments between the divide and the range front consist of two sets: larger catchments that reach the divide, and a smaller set of catchments that are confined to the immediate range front (<2–3 km) and do not reach the main divide. Northeast of the longitudinal drainage, significant topography that likely predates the most recent phase of extension along the Tuzgölü fault zone is underlain by the resistant Cretaceous Ortaköy granitoid (Geological Research Department, 1989b).

The Tuzgölü fault is thought to have initially formed as a normal fault, possibly with a strike-slip component, within a late Maastrichtian continental rift or a large transtensional zone (Görür and Derman, 1978; Görür et al., 1984; Çemen et al., 1999; Derman et al., 2003). Alternatively, it may have formed along a horst during a phase of Neogene extension (Özsayın et al., 2013). Depending on the timing of initiation, the Tuzgölü fault zone may have been reactivated as a strike-slip fault during the Eocene collision of the Tauride and Sakarya continents (Çemen et al., 1999; Robertson et al., 2009), and again during a late Miocene to early Pliocene shortening phase associated with convergence of the African plate (Fernández-Blanco et al., 2013). The Tuzgölü region experienced a changeover from contractional to extensional deformation in the late Miocene to early Pliocene (Özsayin et al., 2013). Paleostress data from the fault zone (Özsayin and Dirik, 2011; Özsayin et al., 2013) and volcanic vents aligned along extensional fractures in the Tuzgölü Basin (Dhont et al., 1998) suggest

Downloaded from https://pubs.geoscienceworld.org/gsa/geosphere/article-pdf/doi/10.1130/GES02175.1/5097193/ges02175.pdf
by guest

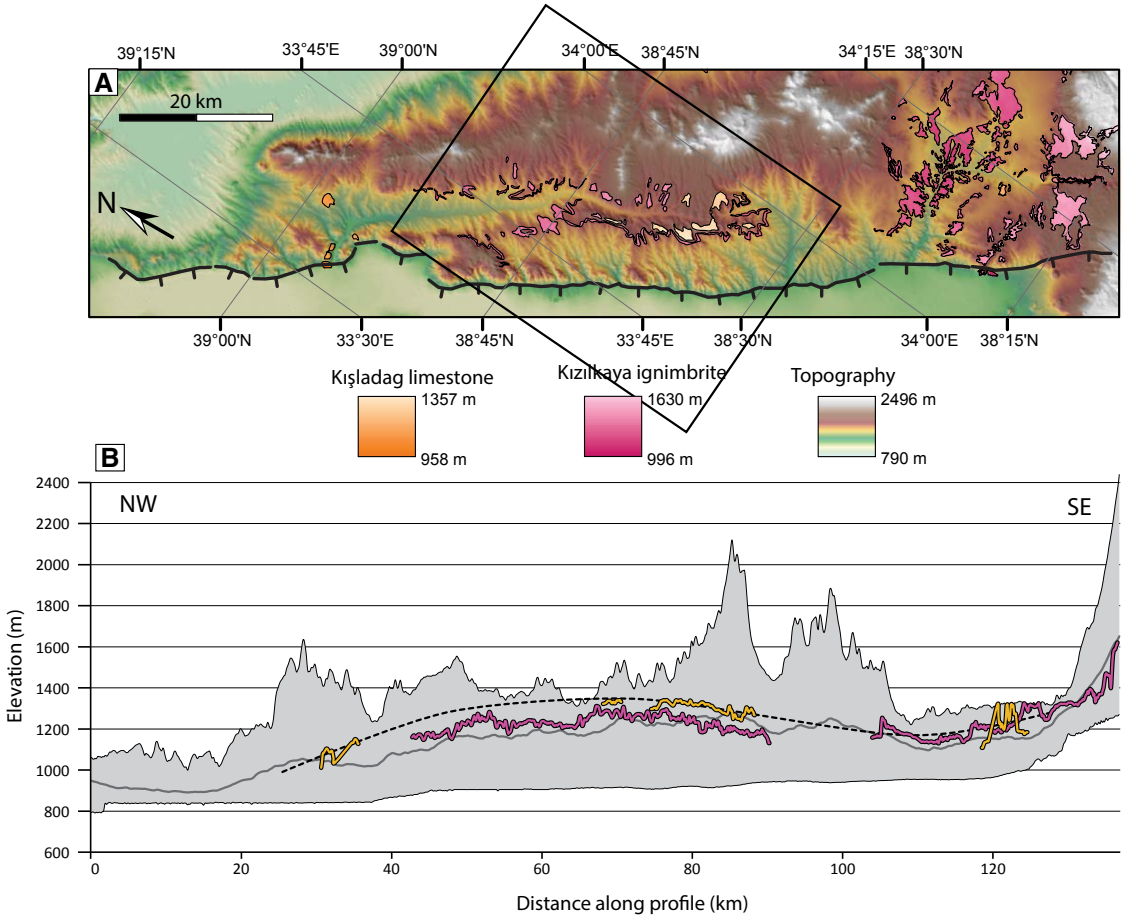

Figure 3. (A) Area encompassed by swath profile in B (see Fig. 5 for location). Major strands of the Tuzgölü fault are shown in black with barbs on the hanging wall. Outcrop patterns of the Kışladağ limestone and Kızılkaya ignimbrite are shown in shades of orange and pink, respectively, shaded by elevation. Black box shows the extent of Figure 4. Topographic base is from U.S. Geological Survey (2019). (B) Swath profile parallel to the long axis of the area shown in A (325° azimuth). Median elevation is shown by the dark gray line, with the area between minimum and maximum elevation bounds shaded light gray. Elevation of the Kışladağ limestone and Kızılkaya ignimbrite are indicated by orange and pink lines, respectively. Black dashed line indicates the approximate regional warping pattern. There are no obvious discontinuities along the length of the swath profile.

that the fault has accommodated northeast-southwest to east-west extension since the early Pliocene.

Presently, the Tuzgölü fault is an extensional system with a possible, poorly constrained right-lateral component (Çemen et al., 1999; Derman et al., 2003; Koçyiğit and Özacar, 2003; Özsayin et al., 2013). The right-lateral component is suggested by dextral focal mechanisms derived from M_w 5.2 and 5.7 earthquakes that occurred ~30 km northwest of the northwestern tip of the Tuzgölü fault in 2005 and 2007, respectively (Fig. 2). However, these earthquakes were located along the along-strike but distinct Bala fault system (Ekström et al., 2012; Emre et al., 2018). A right-lateral component is also argued for based on apparent offset of the Hasan Dag volcano to the west of the Tuzgölü fault zone relative to the nearest major volcanic center to the east (Toprak, 1998). Vertical uplift rates along the Tuzgölü fault zone are 0.08–0.13 mm/yr since 3–5 Ma near the center of the fault zone, based on offset Pliocene lacustrine limestones (Özsayin et al., 2013). Near the southern end of the fault zone, the vertical uplift rate is lower, only at least 0.05 mm/yr, based on offset of the Kızılkaya ignimbrite (Kürçer and Gökten, 2012). Block modeling of GPS data yields higher short-term rates of 1.2 mm/yr vertical and 4.7 mm/yr right-lateral movement in the southeast (Aktuğ et al., 2013). Based on seismic reflection data and deformed lacustrine shorelines, Özsayin et al. (2013) suggested that the main strand of the Tuzgölü fault zone has not been active in the Holocene, but rather has migrated basinward to the Hamzalı fault, or that tectonic displacements are occurring more frequently on the Hamzalı fault. This is evidenced by an ~1.5-m-high scarp along the western flank of the Şereflikoçhisar

Downloaded from https://pubs.geoscienceworld.org/gsa/geosphere/article-pdf/doi/10.1130/GES02175.1/5097193/ges02175.pdf
by guest

Peninsula, whereas 2–8-k.y.-old alluvial fans along the Tuzgölü fault are not transected (Özsayin et al., 2013).

METHODS

In this study, we exploit different temporal and spatial sensitivities to a variety of structural and geomorphic techniques to capture evolving deformation patterns along the Tuzgölü fault system. Pliocene-aged marker beds constrain the longest-term deformation. Geomorphic observations and analysis of river longitudinal profiles from catchments that reach from the fault to the main drainage divide capture deformation that is more recent, in the last few million years. Finally, morphometric analysis of small (>10 km^2) basins immediately adjacent to the Tuzgölü and Hamzalı faults record the most recent (<~1 Ma) and spatially limited (within ~8 km of the fault) patterns of deformation.

Marker Beds

We constrain the geometry of two key marker beds in order to investigate deformation in the footwall of the Tuzgölü fault zone since the Pliocene. The lower marker bed is a 5–10-m-thick ignimbrite locally referred to as the "white ignimbrite level" (5.02 ± 0.2 Ma [^{40}Ar/^{39}Ar]; Özsayin et al., 2013), likely equivalent to the regionally widespread Kızılkaya ignimbrite (5.11 ± 0.37 Ma [U-Pb zircon] or 5.19 ± 0.07 Ma [^{40}Ar/^{39}Ar]: Aydar et al., 2012; 5.46 ± 0.06 Ma [plagioclase^{40}Ar/^{39}Ar]: Lepetit et al., 2014). The ignimbrite is interlayered with fluvial clastic and shallow lacustrine deposits, suggesting it would have draped a landscape with minimal relief at that time (Özsayin et al., 2013), although some initial topography to the marker bed is possible. A lower, pinkish-white ignimbrite layer is also present in the footwall of the Tuzgölü fault zone, with an age of 6.81 ± 0.24 Ma (Özsayin et al., 2013). Due to limited exposure of the lower ignimbrite unit, we do not include it in our analysis, but given its age and stratigraphic position, it can be used to determine a local sedimentation rate of 0.08 mm/yr between deposition of the two ignimbrites. The upper marker bed is a distinctive, 2–10-m-thick lacustrine carbonate unit known as the Kışladağ limestone, which is commonly the last member to have been deposited over the footwall. Assuming that the sedimentation rate of 0.08 mm/yr remained constant after deposition of the Kızılkaya ignimbrite, the Kışladağ limestone would have been deposited at ca. 3.7 Ma (Meijers et al., 2019). The deposition of the Kızılkaya ignimbrite occurred in the early Pliocene, like other lacustrine carbonates of the Central Anatolian Plateau. Limited study of freshwater ostracoda fauna found in the limestone indicates a compatible age of ca. 3 Ma (Tunoğlu et al., 1995; Beker, 2002).

In order to constrain the extent and geometry of these marker beds, we identify their outcrop pattern from digitized 1:100,000-scale Turkish geologic maps (Geological Research Department, 1989a, 1989b, 1990; Dönmez and Akçay, 2005; Dönmez et al., 2005; Akçay et al., 2008). These important regional marker beds are well exposed in the field and therefore accurately captured by these maps. We convert marker bed polygons to elevation data by clipping out segments of a hydrologically corrected, Shuttle Radar Topography Mission (SRTM)–based digital elevation model (DEM) (U.S. Geological Survey, 2019) in a Universal Transverse Mercator projection (World Geodetic System 1984 reference frame) with a cell size of ~110 m (Fig. 3A). We seek to capture along-strike variation in deformation along the Tuzgölü fault system. Therefore, we define a swath box 130 km long, with a long axis orientated 325°, parallel to the trace of the fault system (Fig. 3A). Although there is a slight across-strike dip to the marker beds of ~0.5° toward the northeast, we choose a 30-km-wide swath box to capture the available outcrops of the Kızılkaya ignimbrite and Kışladağ limestone in the footwall of the Tuzgölü fault. We find the maximum, minimum, and mean elevation for the entire landscape and the mean elevation of the outcrop traces of both marker beds (Fig. 3B). We plot the traces of the marker beds in an absolute reference frame, rather than relative to height above the trace of the modern fault, because we are seeking to capture deformation of originally subhorizontal surfaces.

Regional Geomorphology

We make geomorphic observations about the drainages within the footwall of the Tuzgölü fault using a slope map derived from an Advanced Land Observing Satellite (ALOS) DEM (AW3D30 version 2.2, Japan Aerospace Exploration Agency; https://www.eorc.jaxa.jp/ALOS/en/aw3d30/) with a resolution of 30 m (Fig. 4). This map highlights drainages, potential wind gaps, relative levels of incision, and the presence of cliffs around the Kızılkaya ignimbrite and Kışladağ limestone marker beds.

River Longitudinal Profile Analysis

Normalized steepness index (k_{sn}) is the steepness of a longitudinal stream profile channel normalized for contributing catchment area (Whipple and Tucker, 2002). Variations in k_{sn} may be caused by changes or varying patterns of uplift rate, as well as lithologic contrasts (e.g., Cyr et al., 2014; Duvall et al., 2004; Hack, 1957), precipitation rate (e.g., Bookhagen and Strecker, 2012), and stream capture (Robl et al., 2017). Despite complexities, channel steepness values have been successfully used in many studies to infer patterns of uplift along fault systems (e.g., Cyr et al., 2010; Kirby et al., 2003).

Knickpoints are breaks in slope separating graded channel segments. They can be stationary if located along faults or contrasting lithologic units. However, knickpoints can also be transient, caused, for example, by base-level fall or a temporal increase in uplift rate along a fault, and hence their existence can be used to infer a change in tectonic conditions (e.g., Blum and Törnqvist, 2000; Schoenbohm et al., 2004; Whittaker et al., 2008; Walsh et al., 2012; Kent et al., 2017). Transient knickpoints typically take the form of a slope-break knickpoint,

Downloaded from https://pubs.geoscienceworld.org/gsa/geosphere/article-pdf/doi/10.1130/GES02175.1/5097193/ges02175.pdf
by guest

meaning they separate graded segments with different steepness (Kirby and Whipple, 2012). They also tend to migrate upstream as a kinematic wave (Rosenbloom and Anderson, 1994) until slopes along the entire channel have equilibrated (Weissel and Seidl, 1998; Whipple and Tucker, 1999; Niemann et al., 2001). Assuming spatially uniform rock erodibility, precipitation, and uplift rate, the elevation of transient knickpoints initiated at the same time are therefore expected to reflect the relative magnitude of the tectonic perturbation (Niemann et al., 2001; Wobus et al., 2006; Whittaker and Boulton, 2012).

To calculate channel steepness, we follow the methods of Wobus et al. (2006). We analyze 30-m-resolution Advanced Spaceborne Thermal Emission and Reflection Radiometer (ASTER) DEM data (JPL, 2004) using a *Stream Profiler* add-in for ArcGIS software (Geomorphtools, http://geomorphtools.geology.isu.edu/Tools/StPro/StPro.htm) to compute and plot normalized steepness indices and knickpoints. We identify knickpoints visually as breaks both in the river longitudinal profile and in log-transformed slope-area plots. We compute values for k_{sn} through linear regression of segments of the log-transformed slope-area plots. For river longitudinal profile analysis, we focus on the larger set of catchments (>5 km²) that reach the main drainage divide, because smaller catchments (<10 km²) are captured by our morphometric analysis (see the Morphometric Indicators section). Only two of these 23 catchments overlap with catchments analyzed for other morphometric indices (Figs. 5 and 6).

Morphometric Indicators

We perform morphometric analysis of catchments along ~150 km of the Tuzgölü fault and the Hamzalı fault to obtain qualitative information regarding active tectonics in the region from ASTER 30 m DEM data (JPL, 2004). Analysis was restricted to the set of smaller catchments (0.5 km² to 10 km²) in the footwall of the Tuzgölü and Hamzalı faults, resulting in 104 catchments with good spatial coverage along the length of the fault (Fig. 6; Table S2 in the Supplemental Material[1]). Catchments <0.5 km² were excluded because they are dominated by diffusive, colluvial processes. Restricting the analysis to catchments <10 km² ensures that catchments are confined to within 2–3 km of each fault, so their topographic development is largely dominated by recent growth of relief along the Tuzgölü and Hamzalı faults. We exclude six catchments because they consist of two equal-sized branches and cannot be easily interpreted for indices such as asymmetry factor. We exclude an additional six catchments along major fault stepovers. We therefore present data for 92 remaining catchments that span the length of the fault zone. We stop our analysis near the village of Yuva (Fig. 6) because southeast of this point, the fault follows a river rather than the range front, making morphometric relationships more difficult to interpret. The Hamzalı fault forms an escarpment only over a short distance, but it continues as a buried active fault beneath the Tuzgölü salt lake according to seismic reflection data (Fernández-Blanco et al., 2013). However, because the escarpment is strongly expressed only along the southwestern margin of the Şereflikoçhisar Peninsula, we confine our analysis to this segment, excluding catchments altered by salt mining operations on the shore of the peninsula. Morphometric data collected include mountain-front sinuosity (S_{mf}), catchment elongation ratio (E_R), catchment hypsometric integral (*HI*), catchment asymmetry factor (*AF*), and catchment-fault azimuth (A_{cf}). With the exception of S_{mf} (Yıldırım, 2014), these morphometric indices have not been previously measured in the Tuzgölü region.

Mountain-front sinuosity (S_{mf}) is the sinuous length of the mountain front divided by the length of the fault segment trace. It reflects the balance between tectonic forces that produce linear escarpments and erosional forces that cut

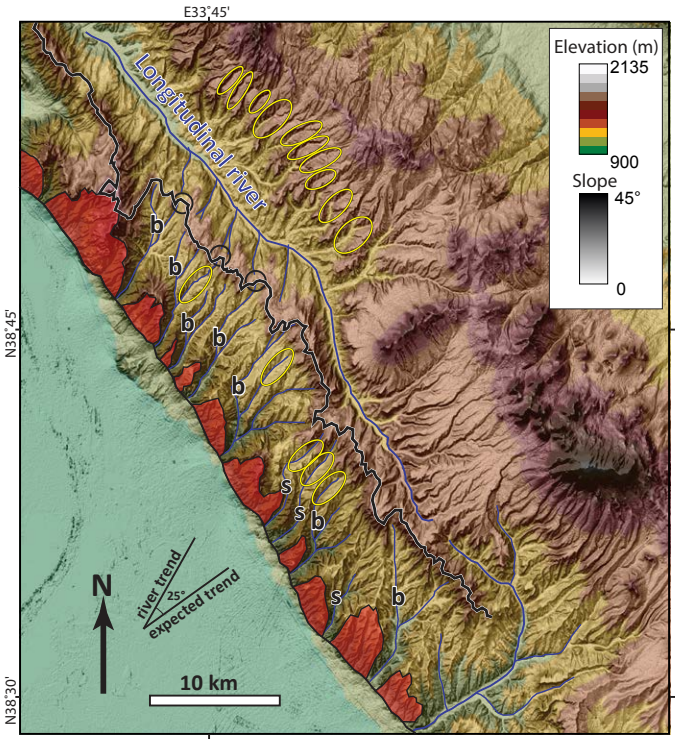

Figure 4. Regional geomorphology showing combination of slope in grayscale with elevation in color; note that there is no shading. Tuzgölü fault is indicated with a black line along the range front. Red polygons denote catchments used in the morphometric analysis, restricted to the immediate footwall of the fault. Drainage network is marked in blue, including a northwest-flowing longitudinal river in the footwall of the fault. S-shaped rivers are marked with "s", and barbed rivers are marked with "b". Yellow ovals indicate asymmetric tributaries, with steeper, shorter drainages to the northwest. Drainage divide between the range front and longitudinal river is marked by heavy black line outlined in white. Note the alignment of drainages across the divide; three potential wind gaps are marked by black circles. Overall trend of rivers is rotated ~25° from the expected trend.

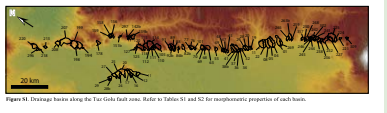

[1]Supplemental Material. Includes map and tables for all morphometrically analyzed basins and river profiles for the 23 analyzed basins. Please visit https://doi.org/10.1130/GEOS.S.12574148 to access the supplemental material, and contact editing@geosociety.org with any questions.

Downloaded from https://pubs.geoscienceworld.org/gsa/geosphere/article-pdf/doi/10.1130/GES02175.1/5097193/ges02175.pdf
by guest

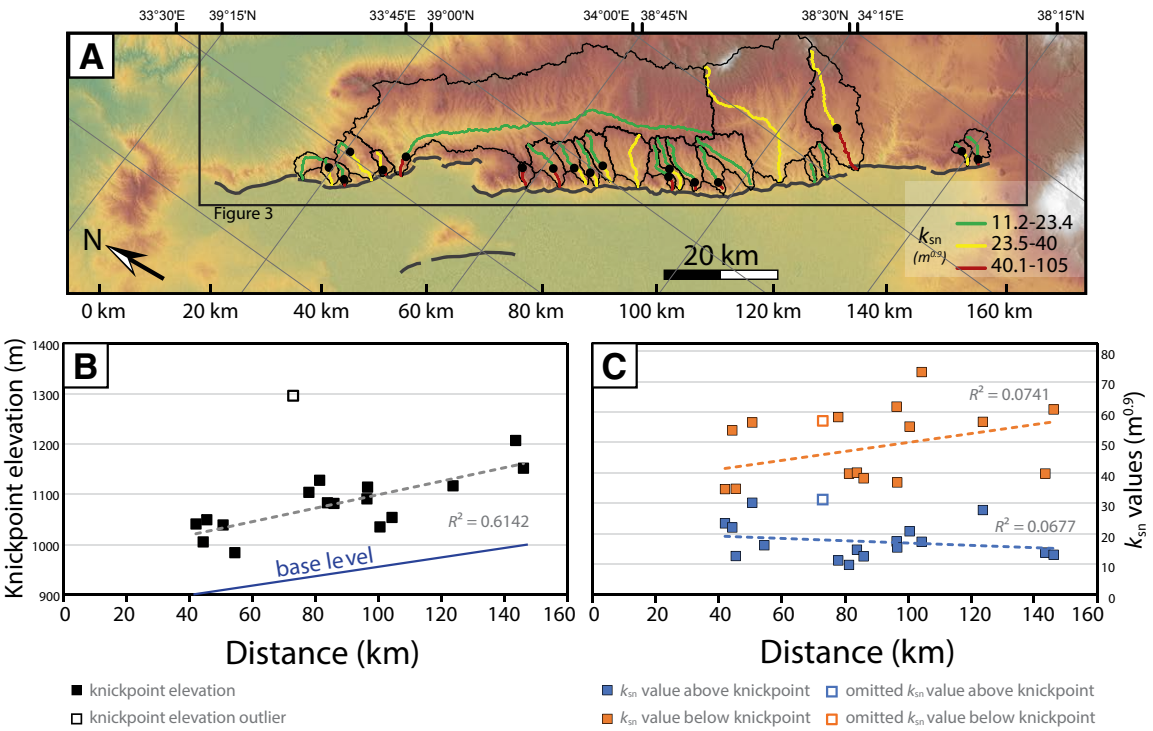

Figure 5. Compiled river profile data (see Figs. S3–S25 [footnote 1] for profiles for each catchment). (A) Map showing traces of the Tuzgölü and Hamzalı faults (thick gray lines) and drainage basins used for river profile analysis (black lines). Rivers are color coded by steepness index (k_{sn}), with knickpoints marked by black dots. Black box indicates the extent of Figure 3. (B) Knickpoints along river profiles, plotted from northwest to southeast; note the increase in elevation to the southeast that roughly corresponds to the increase in base level. Open square is an outlier, omitted from the regression. (C) Channel steepness (k_{sn}) plotted from northwest to southeast, with blue squares for values above the knickpoints and orange squares for values below. Open squares indicate data omitted from regression because of significantly larger drainage area (see panel B). Distance (km) on the *x*-axes of B and C corresponds to that in A.

into the mountain front and reduce relief (Bull and McFadden, 1977). Cessation of faulting, reduction in activity, or high erosion rates would produce an increasingly irregular mountain front and increase S_{mf}, whereas greater uplift rates and more resistant lithologies would produce lower values. Mountain-front sinuosity lower than 1.4–1.6 generally reflects active faulting (Bull and McFadden, 1977; Small and Anderson, 1998), although this is complicated by lithologic resistance (weaker rocks are more easily eroded, increasing S_{mf}), high sedimentation rates (retreat of fan apexes into the footwall under high sedimentation increases S_{mf}), and the scale of the map (lower S_{mf} is obtained from maps with coarser resolution). We trace fault-bounded escarpments in the region using 30-cm- and 50-cm-resolution DigitalGlobe WV01 panchromatic and WV02 multispectral satellite imagery (https://gbdxdocs.digitalglobe.com/docs/worldview-2). We find that slopes of more than ~15° generally correspond to bedrock, and so use this value to help us define the mountain front. We divide the Tuzgölü fault into eight segments and the Hamzalı fault into two segments based on major stepovers and fault linkages, producing an S_{mf} value for each segment.

The elongation ratio (E_R), or the aspect ratio of catchments, may reflect relative tectonic uplift rate or lithology. Elongation ratio (E_R) is calculated using the following equation:

$$E_R = \frac{2\sqrt{S/\pi}}{L}, \quad (1)$$

where S is catchment area and L is the length of the catchment (Schumm, 1956). This equation compares the area of a catchment to a circle with a diameter

Downloaded from https://pubs.geoscienceworld.org/gsa/geosphere/article-pdf/doi/10.1130/GES02175.1/5097193/ges02175.pdf
by guest

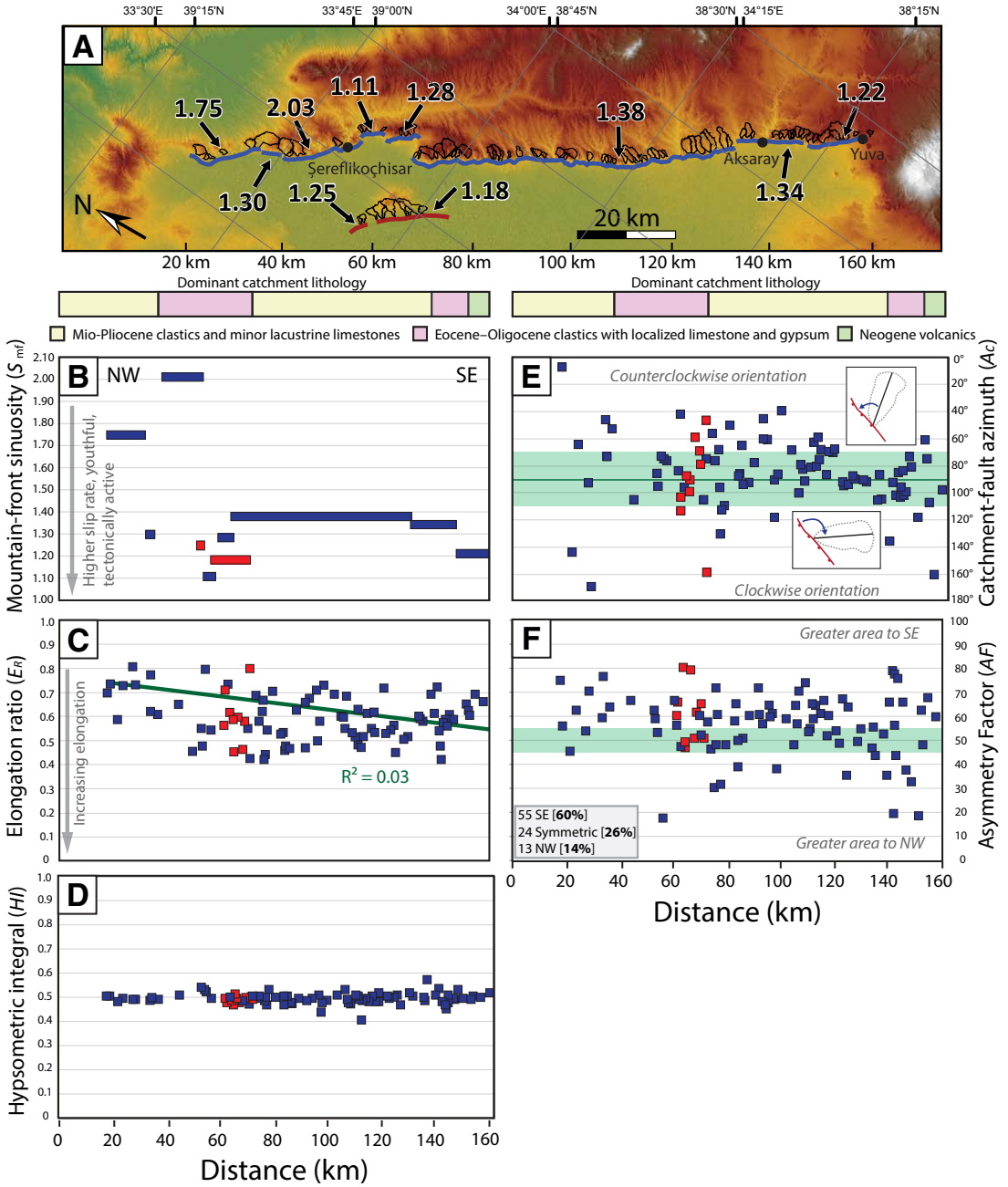

Figure 6. Morphometric data. (A) Map showing mountain-front sinuosity (S_{mf}) of fault-bounded escarpments of the Tuzgölü (blue) and Hamzalı (red) faults, as well as drainage basins used for our morphometric analysis. White values indicate S_{mf} indices for corresponding fault segments. Fault-bounded escarpments were traced from DigitalGlobe, Inc., WV01 panchromatic 30-cm- and 50-cm-resolution satellite imagery. Map was generated using Advanced Spaceborne Thermal Emission and Reflection Radiometer (ASTER) 30 m digital elevation model data (JPL, 2004). (B–F) Morphometric data for segments of the Tuzgölü (blue) and Hamzalı (red) faults plotted from northwest to southeast. Dominant catchment lithology can be seen above the respective geomorphic index plots. Distance (km) on the *x*-axes corresponds to that in A.

Downloaded from https://pubs.geoscienceworld.org/gsa/geosphere/article-pdf/doi/10.1130/GES02175.1/5097193/ges02175.pdf
by guest

equal to the length of the long axis of the catchment. Values for E_R range from 0 to 1, where circular catchments have E_R values close to 1, and E_R approaches 0 for increasingly elongate catchments. On newly exposed, planar surfaces such as fault scarps, drainages are initially closely spaced and parallel, with narrow, elongate catchments; as incision proceeds, they progressively evolve to more dendritic networks, delimited by catchment boundaries with lower aspect ratios (Densmore et al., 2005). Low E_R corresponds with catchments in their early stage of development or where uplift rate is high relative to watershed migration, such that downstream elongation proceeds quickly compared to enlargement (Suresh, 2000; Sólyom and Tucker, 2007). Evolved catchments are more variable in shape and exhibit a combination of elongated and circular morphologies due to dominance of catchment integration over tectonic uplift (Hancock and Willgoose, 2001; Densmore et al., 2004). More resistant lithology results in catchments that retain their elongated shape over longer periods, whereas more easily erodible lithologies evolve to variable catchment morphologies more quickly.

Hypsometry is the relationship between elevation and catchment area (Langbein, 1947; Strahler, 1952; Schumm, 1956). Hypsometric curves represent cumulative basin area versus elevation and can be utilized to calculate hypsometric integrals (*HI*), which reflect catchment relief. The shape of the hypsometric curve is independent of differences in catchment size, allowing catchments of varying sizes to be compared (Strahler, 1952). A convex-up hypsometric curve indicates that more of the catchment area consists of relatively higher elevations. This is commonly attributed to recent uplift to which catchments have not yet equilibrated (Strahler, 1952; Schumm, 1956; Keller and Pinter, 2002). A concave-up hypsometric curve indicates that a majority of catchment area lies at relatively low elevations in a degrading, inactive landscape (Strahler, 1952; Schumm, 1956; Keller and Pinter, 2002). S-shaped or linear hypsometric curves are commonly interpreted to reflect a catchment that is in dynamic equilibrium (Keller and Pinter, 2002). Hypsometric integral (*HI*) is calculated with the following equation:

$$HI = \frac{(h_{mean} - h_{min})}{(h_{max} - h_{min})}, \quad (2)$$

where h_{mean} is the mean of the elevations within the catchment, and h_{max} and h_{min} are the maximum and minimum elevations within the basin, respectively (Strahler, 1952; Pike and Wilson, 1971). Catchments with *HI* values of <0.30 are considered to reflect little to no active uplift, whereas *HI* values >0.60 indicate unstable, actively uplifting catchments, or those adjusting to a new tectonic regime (Strahler, 1952; Keller and Pinter, 2002).

Tectonic deformation can cause catchments to become asymmetric, with a greater area on one side of the trunk stream or the other. The degree of this asymmetry can be captured by measuring the catchment asymmetry factor (*AF*), which is calculated as $100 \times (A_R/A_T)$, where A_R is the area to the right of the trunk stream in the upstream direction and A_T is the total area of the catchment (Hare and Gardner, 1985). Following previous studies, we prescribe classes to quantify asymmetry of catchments, where $45 < AF < 55$ reflects a symmetric catchment; $AF > 55$ reflects a greater proportion of the drainage area to the right of the trunk stream, which in this case is to the southeast; and $AF < 45$ reflects the opposite with greater area to the left, or northwest. As the *AF* value deviates from the central value in either direction, the potential influence of tectonic tilting increases accordingly (Keller and Pinter, 2002; Özkaymak and Sözbilir, 2012).

Finally, tectonic deformation may also be reflected in the angle between the long axis of a catchment and the bounding fault, with deviations from an orthogonal relationship implying tilting or large-scale shearing. We measured the orientation of catchments relative to the Tuzgölü and Hamzalı faults. To determine orientation, we use the minimum bounding geometry (MBD) in ArcGIS, which is defined as the minimum bounding rectangle that can be fit to the catchment. The long axis of the basin (the basin orientation) is delineated by finding the greatest distance between two points within the MBD feature. We define a morphometric factor we call catchment-fault azimuth (A_{cf}), which is the angle between the fault and the main axis of the catchment measured in a counterclockwise direction. We consider catchments that display angles <70° to be oriented clockwise relative to the fault, and angles >110° to be oriented counterclockwise. Catchments that fall between 70° to 110° are approximately orthogonal to the fault.

RESULTS

Marker Beds

Swath profiles of the mapped outcrop pattern of footwall marker beds capture deformation parallel to the trace of the Tuzgölü fault since ca. 3.7 Ma. Both the Kızılkaya ignimbrite and Kışladağ limestone marker beds form relatively smooth features in the study region. Minor high-frequency variation in the altitude of the marker beds along strike of the swath profiles (Fig. 3B) is likely attributable to mismatches between the precision of the mapping and the scale of the DEM. The two marker beds are consistently spaced, with the Kışladağ limestone projecting ~100 m above the Kızılkaya ignimbrite (Fig. 3B). Both units form a broad arch centered on approximately the center of the Tuzgölü fault zone. The ignimbrite shows a second increase in elevation at the southeastern end of the swath profile, but exposures of the limestone are too sparse to determine whether they similarly increase in elevation. Long-wavelength topography roughly parallels the deformation of the marker beds, while shorter-wavelength variations are due to residual peaks made of Cretaceous Ortaköy granitoid rocks (Geological Research Department, 1989b) protruding above the sediment fill (especially ~90–130 km along the profile; Fig. 3B).

Regional Geomorphology

Based on our observations of the regional geomorphology (Fig. 4), we note that tributaries appear to align across the divide separating the Tuzgölü Basin

Downloaded from https://pubs.geoscienceworld.org/gsa/geosphere/article-pdf/doi/10.1130/GES02175.1/5097193/ges02175.pdf
by guest

from the longitudinal river ~10 km to the northeast. Rivers southwest of the divide between the range front and the longitudinal river that drain directly into the Tuzgölü Basin, as well as tributaries that flow into the longitudinal river from both the northeast and southwest, follow the same trend, with an orientation of ~N30°E. Note that this trend is not perpendicular to the trend of the Tuzgölü fault, but rather is rotated ~25° counterclockwise with respect to the trend of the fault (Fig. 4). Erosion along tributaries is commonly asymmetric; southeast-facing slopes tend to be shorter and more gullied, whereas northwest-facing slopes are longer and less incised (marked with yellow ovals in Fig. 4). This effect is more pronounced on tributaries that run east-northeast compared to north-northeast. Rivers southwest of the divide that drain into the Tuzgölü Basin are in some cases S-shaped (marked with "s" in Fig. 4) or consist of two or more major branches that collect into the southeasternmost drainage (marked with "b" in Fig. 4). We note three possible wind gaps (marked with black circles in Fig. 4) between aligned tributaries on either side of the divide, marked by a low spot in the ridgeline.

River Longitudinal Profile Analysis

Of the river profiles from the 23 catchments analyzed, 17 yielded knickpoints (Fig. 5A; Figs. S3–S23 [footnote 1]). The knickpoints are slope-break type (Kirby and Whipple, 2012), separating regions of higher k_{sn} below from lower k_{sn} above (Figs. 5B and 5C), and do not clearly lie along mapped lithologic boundaries (Figs. S3–S23). We exclude as an outlier the knickpoint at 1300 m elevation, which is ~200 m higher than its nearest neighbor. For the remaining 16 knickpoints, elevation increases by 140 m to the southeast (Fig. 5B). However, base level also increases by 100 m along this same distance (Fig. 5B).

Compared to other active tectonic settings, k_{sn} values in rivers both above and below the knickpoints are low (<75 $m^{0.9}$), suggesting either relatively low rates of uplift or highly erodible lithology (Fig. 5C; Figs. S3–S23 [footnote 1]). Values of k_{sn} are ~2×–6× higher below compared to above the knickpoints. The upper segments display k_{sn} in the range of 10–20 $m^{0.9}$, decreasing in value toward the southeast. In contrast, the segments below the knickpoints are steeper, with k_{sn} values ranging from 40 to 60 $m^{0.9}$. River steepness values below the knickpoints are increasingly higher to the southeast (Fig. 5C).

Morphometric Indicators

All but two of the 10 segments along the Tuzgölü fault zone have mountain-front sinuosity (S_{mf}) values <1.4 (Figs. 6A and 6B), in the range of values reflecting active faulting (Bull and McFadden, 1977; Small and Anderson, 1998). Along the Tuzgölü fault, S_{mf} values decrease from 1.75–2.03 in the northwest to 1.23 in the southeast, but this trend is punctuated by lower values (as low as 1.1) near the town of Şereflikoçhisar where the fault steps back into the range. S_{mf} values are also low (1.18–1.25) along the Hamzalı fault. In terms of elongation ratio (E_R), elongated catchments are more common along the central and southeastern Tuzgölü fault zone, with E_R ranging from 0.4 to 0.75 (75–160 km in Fig. 6C). In contrast, catchments show increasingly circular morphologies toward the northwest, confined to E_R of ~0.6–0.8 in the far northwest (0–45 km in Fig. 6C). We observe a range of E_R values along the Hamzalı fault (0.45–0.80). These values follow the general trend of E_R along the Tuzgölü fault. Hypsometric integral (*HI*) values range from 0.48 to 0.63 with a mean *HI* of 0.50 for the Tuzgölü fault, and 0.46 to 0.52 with a mean of 0.48 for the Hamzalı fault (Fig. 6D). There is no spatial trend to the hypsometric data.

Analysis of catchment asymmetry factor (*AF*) reveals that of the 92 catchments in the study area, 60% exhibit greater area to the southeast, 14% exhibit greater area to the northwest, and 26% are classified as symmetric (Fig. 6F). The strongest signal of asymmetry is along the Hamzalı fault and the middle and northwestern sectors of the Tuzgölü fault (0–120 km on Fig. 6F). Although the Tuzgölü fault southeast of Aksaray is still dominated by asymmetric catchments, we also observe an increase in variability of basin symmetry in this region. This variability coincides with a change in lithology from moderately to weakly consolidated Mio-Pliocene continental clastics to Oligocene clastics and Plio-Quaternary volcanics. We observe a similar trend in catchment-fault azimuth (A_{cf}) as well. Most of the catchments in the Tuzgölü region are oriented orthogonal to the fault (Fig. 6E). However, more catchments have a counterclockwise orientation (23 total, or 25%), compared to clockwise (10 total, or 11%). There is no clear spatial trend along the fault.

DISCUSSION

We observe three distinct patterns of deformation in our structural and geomorphic data: (1) a Pliocene phase of deformation that resulted in uplift along the central part of the Tuzgölü fault; (2) a more recent shift to higher uplift rates along the southeast part of the Tuzgölü fault; and (3) regional northward tilting. We explore the evidence for each of these in turn, followed by a discussion of implications for regional tectonics. We close this section with a short exploration of how our study informs recent fault activity and determination of regional seismic hazards.

Spatial and Temporal Patterns of Deformation along the Tuzgölü Fault Zone

Sensitive to longer time scales, mapping of the Kışladağ limestone and Kızılkaya ignimbrite indicates deformation into a broad arch with a maximum uplift of ~300 m in the central part of the footwall of the Tuzgölü fault zone (Fig. 3B). This deformation must have begun at or after ca. 3.7 Ma, the age of the Kışladağ limestone (Meijers et al., 2019), the upper marker bed. The three wind gaps we observe in the footwall of the fault would have formed at this time, as the existing drainage network was disrupted by uplift. Topographic

Downloaded from https://pubs.geoscienceworld.org/gsa/geosphere/article-pdf/doi/10.1130/GES02175.1/5097193/ges02175.pdf
by guest

elevations are also highest in the central part of the footwall (as also noted by Yıldırım [2014]), and in the adjacent hanging wall, well data indicate greatest thickening of Plio-Quaternary fluvio-lacustrine deposits (Gürbüz and Kazancı, 2014). This pattern of along-strike footwall deformation in the central Tuzgölü fault zone is characteristic of the displacement geometry for normal faults (Dawers et al., 1993). From our data we can calculate maximum displacement (D_{max}) versus fault length (L) ratios of 0.041 for the Kışladağ limestone and 0.071 for the Kızılkaya ignimbrite, within the range of values typical of normal faults ($D_{max}/L = 10^{-1}$ to 10^{-3}; Kim and Sanderson, 2005).

We observe a single knickpoint in most streams we analyzed (Fig. 5). These knickpoints are of the slope-break type (Kirby and Whipple, 2012), separating regions of higher and lower k_{sn}. Although the knickpoints climb in elevation by ~140 m from northwest to southeast, base level increases ~100 m over the same distance (Fig. 5B). Knickpoints do not clearly lie on mapped lithologic boundaries. We argue that based on their morphology and distribution, the knickpoints are transient and could reflect a change in climatic or tectonic forcing. We rule out a significant climatic trigger for knickpoint formation because the region has been semiarid since at least 5 Ma, based on carbon ($\delta^{13}C$) and oxygen ($\delta^{18}O$) isotopes from lake carbonates (Meijers et al., 2018). Rather, a change in uplift rate (or pattern) or tectonically induced base-level fall along the Tuzgölü fault is the most likely culprit for knickpoint formation.

River profile and morphometric data indicate that the change that initiated the transient knickpoints corresponds to a pattern of more significant uplift toward the southeastern part of the Tuzgölü fault. River steepness values (k_{sn}) below the knickpoints increase to the southeast from 35 to 60 $m^{0.9}$ (Fig. 5C), 2×–6× higher than k_{sn} values above the knickpoints. Mountain-front sinuosity (S_{mf}) also decreases to the southeast from values as high as ~2 to a low of 1.2 at the southeastern end of the fault (Figs. 6A and 6B). This decrease implies either that the fault is uplifting at a higher rate there, or that it is younger and actively propagating toward the Hasan Dag volcano. In an exception to this trend, fault segments near the town of Şereflikoçhisar in both the Hamzalı and northwestern Tuzgölü escarpments exhibit low S_{mf} indices, substantially lower than the mean for the Tuzgölü range front, suggesting locally elevated tectonic activity. These locally low values could reflect basinward migration of deformation and fault interaction, a topic we return to at the end of this section. Basin elongation (E_R) data show a similar trend of decreasing values (increasing elongation) to the southeast along the Tuzgölü fault (Fig. 6C). The presence of circular basin geometries in the northwest indicates lower uplift rates or more evolved catchments. Catchments are increasingly elongated toward the central and southeastern Tuzgölü fault zone, suggesting higher uplift rates toward the southeast or a southeastward-propagating fault. Interestingly, hypsometric data (*HI*) show no along-strike trend (Fig. 6D). A change in fault uplift rate to the southeast is also supported by modest deformation of the Kızılkaya ignimbrite marker bed (Fig. 3B). However, the sparse outcrops of the Kışladağ limestone make it difficult to know how much of the marker-bed morphology in the southeast reflects preexisting topography versus deformation.

Our observations imply higher uplift rate, base-level fall, more recent fault activity (southeastward propagation), or more resistant lithology to the southeast along the Tuzgölü fault. The latter can be discarded because there is no abrupt change in indices associated with the change in lithology from Mio-Pliocene clastics to relatively more resistant Oligocene clastics and Plio-Quaternary volcanics southeast of Aksaray. The trends are gradual and unrelated to lithologic boundaries (Figs. 2 and 6). The increase in river steepness (k_{sn}) to the southeast (Fig. 5) is also strong evidence for a higher uplift rate or sustained base-level fall rather than fault propagation, because k_{sn} is inferred to be a function of uplift rate (Wobus et al., 2006) and a propagating fault does not necessarily experience different uplift rates along strike. Finally, we find a change in uplift rate more likely than base-level fall, given the evidence for recent activity along the Tuzgölü fault. Therefore, our morphometric data suggest higher uplift rate to the southeast along the Tuzgölü fault. The timing of the shift from highest uplift rate in the center of the footwall to higher uplift rate in the southeast is unknown. Other studies have found that rivers retain transient signals such as these over 1–3 m.y. time scales (e.g., Whittaker et al., 2008). Given the relatively small size of our studied basins (which could adjust quickly), the transition may have occurred at the low end of this range, but we cannot further quantify the timing.

In addition to our evidence for changing deformation patterns in the footwall of the Tuzgölü fault, we find consistent evidence for regional north or northwest tilting. Basin asymmetry factor (*AF*) is dominated by catchments with greater areas to the southeast of the trunk stream, suggesting rivers are migrating laterally to the northwest as a result of tilting down to the north or northwest (Keller and Pinter, 2002), particularly northwest of Aksaray (Fig. 6F). Additionally, there is a tendency toward a counterclockwise orientation of catchments along the Tuzgölü fault (catchment-fault azimuth [A_{cf}]; Fig. 6E). Orientation of the catchments could reflect rotation due to distributed left-lateral shearing within the footwall of the Tuzgölü fault, which would tend to elongate basins in an approximately north-south orientation. Alternatively, a counterclockwise orientation could reflect north-northwest–directed tilting if the catchment outlet remained pinned, but the catchment overall migrated north or northwest. The similarity of *AF* and A_{cf} along the Tuzgölü and Hamzalı faults suggests regional tilting affecting both the footwall and hanging wall of the Tuzgölü fault zone. Away from the immediate footwall scarp of the Tuzgölü fault zone, drainage patterns can also be explained by north-northwest tilting. Larger rivers that reach the divide are oriented ~25° counterclockwise with respect to the range front and are commonly S-shaped or branching (Fig. 4). This pattern could be similarly explained by large-scale shear in the footwall of the fault or by north to northwest tilting. Finally, asymmetric erosion patterns, with shorter, more deeply dissected south-southeast–facing slopes, suggests north or northwest tilting. Note that we observe asymmetric tributaries on either side of the point of maximum uplift of the footwall strata based on warping of the marker beds (Figs. 3 and 4), indicating a regional tectonic cause rather than local deformation. We discard large-scale shearing in the footwall of the fault as an explanation for these observations because the

Downloaded from https://pubs.geoscienceworld.org/gsa/geosphere/article-pdf/doi/10.1130/GES02175.1/5097193/ges02175.pdf
by guest

implied sense of shear is left-lateral, contrary to observations of right-lateral or pure normal displacement on the modern Tuzgölü fault (Çemen et al., 1999; Derman et al., 2003; Koçyiğit and Özacar, 2003; Özsayin et al., 2013). Therefore, our observations constitute strong evidence for regional tilting to the north or northwest. Unfortunately, we cannot constrain the timing of onset of tilting with our current data.

Finally, we return to the question of basinward migration of deformation as suggested by Özsayin et al. (2013). Our data partially support higher activity along the basinward Hamzalı fault in that mountain-front sinuosity (S_{mf}) indices are lower there compared to along the Tuzgölü fault (Figs. 6A and 6B). However, other morphometric indices for the Hamzalı fault are indistinguishable from those along the Tuzgölü fault (Fig. 6). Thus, our results are inconclusive.

Tectonic Implications

Our data suggest onset of extension along the Tuzgölü fault at ca. 3.7 Ma, consistent with the inference for a regional changeover from contractional to extensional deformation in the late Miocene to early Pliocene (Özsayin et al., 2013). Extension also appears to be coeval with the interior of the Central Anatolian Plateau reaching its present-day elevation (Aydar et al., 2013; Meijers et al., 2018). The Tuzgölü fault zone lies near the transition from compression caused by collision of the Arabian plate to the east, to extension above the Aegean slab to the west (McClusky et al., 2000; Reilinger et al., 2006); the onset of extension could reflect the adjustment of internal blocks during westward translation of the Anatolian block (e.g., Şengör et al., 1985).

Our observations of regional, northward tilting could have a number of explanations. Asymmetric uplift could reflect slab fragmentation and subsequent rebound of the downgoing plate (Duretz et al., 2011; Schildgen et al., 2014; Delph et al., 2017) or isostatic rebound in response to crustal thickening that was suppressed until rollback and detachment of the Cyprus slab (Abgarmi et al., 2017). Arc root removal beneath the Kırşehir block (Göğüş et al., 2017) or delamination of a formerly horizontally subducting slab (Bartol and Govers, 2014) could also have caused uplift and northward tilting in the Central Anatolian Plateau. Without additional data on the regional pattern and timing of tilting, we cannot test among these models.

The change in kinematics recorded by our morphometric data is a previously undescribed phenomenon. It is possible that deep-rooted, slab-related processes drove this change. For example, in Pliocene to younger times, slab necking (Delph et al., 2017), complete slab breakoff (Abgarmi et al., 2017), and/or the arrival of continental fragments like the Eratosthenes seamount into the trench (e.g., Schattner, 2010; Delph et al., 2015) may have led to an acceleration in uplift in the Central Taurides (Schildgen et al., 2012a), and could explain a change in kinematics along the Tuzgölü fault zone. Complex and evolving block rotations in the context of crustal translation away from the Arabian collision and toward the Aegean trench could also explain this change (Şengör et al., 1985). Average bulk counterclockwise rotation of the Central Anatolian Crystalline Complex (Fig. 1C) ranging from 24° to 33° throughout the Eocene and Neogene has been documented in paleomagnetic studies (Tatar et al., 1996; Platzman et al., 1998), and GPS studies calculate present-day 1.2°–1.4°/m.y. counterclockwise rotation of Central Anatolia (McClusky et al., 2000; Ayhan et al., 2003; Aktuğ et al., 2009). Block modeling of GPS data suggests variable behavior along the Tuzgölü fault. Aktuğ et al. (2013) found evidence for short-term deformation rates of 1.2 mm/yr vertical and 4.7 mm/yr right-lateral, but interestingly, right-lateral slip is limited to the middle and southeastern part of the fault. Simão et al. (2016) also found variability in behavior along the fault, with transtension in the northwest and southeast and transpression in the middle. Although neither block modeling–based study is consistent with the geology, their results illustrate the importance of block rotation in imparting variable kinematics along a fault zone.

Alternatively, the shift to higher uplift rates in the southeastern part of the Tuzgölü fault zone may reflect interactions with the Hasan Dag volcano. Although an early stage of volcanic edifice formation is recognized (the 13–7 Ma Keçikalesi paleovolcano; Deniel et al., 1998), major growth occurred after 2.4 Ma (Reid et al., 2017), building the meso- (ca. 1.0–0.15 Ma) and neo–Hasan Dag volcanoes (<0.15 Ma) (Aydar and Gourgaud, 1998; Deniel et al., 1998). The cluster of monogenetic basalts associated with Hasan Dag is also Quaternary in age (Notsu et al., 1995; Şen et al., 2004). The timing and location of major growth of the Hasan Dag volcanic complex therefore coincides with our observed change in kinematics along the Tuzgölü fault. Many studies have documented fault-volcano interactions, though commonly the emphasis is on how faults control the distribution and morphology of volcanic vents and structures (e.g., Mathieu et al., 2011). In the case of the Tuzgölü fault, however, it may be that volcanic emplacement drove localized extension. In New Zealand, for example, higher slip rates along the Rangipo fault are linked to the timing of volcanic eruptions (Villamor et al., 2007), and in Iceland, movement on normal faults is temporally correlated with magmatic events (Bull et al., 2003). These examples, however, refer to changes in rate over shorter time scales than envisaged along the Tuzgölü fault. Alternatively, high heat flow associated with Hasan Dag (Reid et al., 2017, and references therein) may have locally weakened the crust, leading to stress concentration or a decrease in flexural rigidity along the southeastern segment of the fault, resulting in the change in kinematics.

Modern Fault Activity and Seismic Hazards

Presently, the Tuzgölü fault is an extensional system with a possible, poorly constrained right-lateral component (Çemen et al., 1999; Derman et al., 2003; Koçyiğit and Özacar, 2003; Özsayin et al., 2013; Kürçer and Gökten, 2012) and is confirmed active on the basis of paleoseismic studies (Kürçer and Gökten, 2012). Some of our morphometric data confirm that the fault is active. Mountain-front sinuosity (S_{mf}), for example, is <1.4 for most fault segments (Fig. 6B),

Downloaded from https://pubs.geoscienceworld.org/gsa/geosphere/article-pdf/doi/10.1130/GES02175.1/5097193/ges02175.pdf
by guest

indicating "moderate" fault activity with a morphometrically inferred "class 2" uplift rate of between 0.05 and 0.5 mm/yr (Rockwell et al., 1985; Yıldırım, 2014). However, other indicators fail to demonstrate significant activity. Hypsometric integral (*HI*) hovers around the equilibrium value of 0.5, and river-channel steepness (k_{sn}) below the knickpoints, which is adjusted to the most recent phase of uplift, is low, with values all <75 $m^{0.9}$ (Fig. 5C). Our geomorphic observations thus are consistent with low-uplift-rate estimations based on offset of the Kızılkaya ignimbrite, which indicates uplift rates of 0.05–0.13 mm/yr (Özsayin et al., 2013; Kürçer and Gökten, 2012) since ca. 5 Ma. Taken together, evidence indicates that the Tuzgölü fault is active, but uplift rates are relatively low and/or channels adjust quickly to changes to the system because of relatively weak lithology.

Because the Tuzgölü fault is active, it poses some level of seismic hazard. This is confirmed by paleoseismic trenching along the southeastern part of the fault, which suggested potential for M_w 6.7 events with an average recurrence interval of 4664 yr, with the most recent event constrained to 5560–1370 yr B.P. (Kürçer and Gökten, 2012). Fault uplift rates based on offset of the Kışladağ limestones suggest extensional rates of 0.08–0.13 mm/yr in the middle part of the fault zone (Özsayin et al., 2013) and 0.05 mm/yr in the southeast based on offset of the Kızılkaya ignimbrite (Kürçer and Gökten, 2012). However, whereas Yıldırım (2014) suggested that seismic hazard was greatest in the central part of the fault zone, our data show that the seismic hazard is greatest in the southeastern part of the fault, where the recent uplift rate is highest. Therefore, the seismic hazards associated with the Tuzgölü fault remain poorly constrained and warrant further paleoseismic study.

CONCLUSIONS

In this study, we combine observations of regional geomorphology, mapping of key marker beds, and morphometric analysis of drainages along the Tuzgölü fault zone. Deformation of the Kızılkaya ignimbrite and Kışladağ limestone suggests onset of extension with a normal-fault scaling relationship (i.e., greatest displacement near the center of the fault) ca. 3.7 Ma, consistent with the onset of regional extension. We observe evidence for northward regional tilting, suggested by catchment asymmetry, catchment-fault azimuth, and observation of tributary asymmetry in the regional drainage network. Tilting could reflect slab fragmentation, slab delamination, or removal of a lithospheric root.

Our data identify for the first time an important shift in the kinematics of deformation along the Tuzgölü fault after deposition of the Kışladağ limestone (i.e., <3.7 Ma). This shift is marked by the presence of single knickpoints in rivers along the Tuzgölü fault. Higher uplift rates in the southeast are supported by modest upwarping of the Kızılkaya ignimbrite in this area. This more local deformation signal may reflect further evolution within the subducting slab (i.e., final breakoff or additional fragmentation), but could also reflect changes in block rotation or interaction with the Hasan Dag volcano. The timing of the main stage of growth of the volcano along with the spatial correlation with deformation patterns along the Tuzgölü fault support the hypothesis that growth of Hasan Dag may have driven extension along the southeastern part of the fault zone or may have facilitated focused activity by decreasing the regional flexural rigidity. In any case, this previously unrecognized pattern of recent deformation means that seismic hazards associated with the Tuzgölü fault zone are largely unconstrained.

ACKNOWLEDGMENTS

The data for this paper are fully contained in the manuscript and the associated Supplemental Material (footnote 1), including a map and tables for all morphometrically analyzed basins and river profiles for the 23 analyzed basins. Questions may be addressed to the corresponding author. This research was supported by Natural Sciences and Engineering Research Council of Canada Discovery Grant funding to L. Schoenbohm and U.S. National Science Foundation Continental Dynamics–Central Anatolian Tectonics (CD-CAT) proposal 1109703. We thank the entire CD-CAT team for discussion of this work and invaluable insight, and Bulent Tokay for assistance in the field. We also thank Mike Darin for assistance in providing access to ArcGIS geological data. Satellite imagery is copyright DigitalGlobe, Inc., and provided through the Polar Geospatial Center (University of Minnesota–Twin Cities, Saint Paul, Minnesota, USA). We wish to thank David Fernández-Blanco, an anonymous reviewer, and the Geosphere science editor and associate editors for their thorough, thoughtful reviews that significantly improved this contribution.

REFERENCES CITED

Abgarmi, B., Delph, J.R., Ozacar, A.A., Beck, S.L., Zandt, G., Sandvol, E., Trukelli, N., and Biryol, C.B., 2017, Structure of the crust and African slab beneath the central Anatolian plateau from receiver functions: New insights on isostatic compensation and slab dynamics: Geosphere, v. 13, p. 1774–1787, https://doi.org/10.1130/GES01509.1.

Akbaş, B., Akdeniz, N., Aksay, A., Altun, İ.E., Balcı, V., Bilginer, E., Bilgiç, T., Duru, M., Ercan, T., Gedik, İ., Günay, Y., Güven, İ.H., Hakyemez, H.Y., Konak, N., Papak, I., Pehlivan, Ş., Sevin, M., Şenel, M., Tarhan, N., Turhan, N., Türkecan, A., Ulu, Ü, Uğuz, M.F., and Yurtsever, A., compilers, 2011, Geological Map of Turkey, MTA (Mineral Research and Exploration General Directorate), scale: 1:1,250,000, 1 sheet.

Akçay, A.E., Dönmez, M., Kara, H., Yergök, A.F., and Esentürk, K., 2008, Geologic map of the Kırşehir—J30 quadrangle: Ankara, General Directorate of Mineral Research and Exploration of Turkey, scale 1:100,000.

Aktuğ, B., Kiliçoğlu, A., Lenk, O., and Gürdal, M.A., 2009, Establishment of regional reference frames for quantifying active deformation areas in Anatolia: Studia Geophysica et Geodaetica, v. 53, p. 169–183, https://doi.org/10.1007/s11200-009-0011-0.

Aktuğ, B., Parmaksız, E., Kurt, M., Lenk, O., Kılıçoğlu, A., Gürdal, M.A., and Özdemir, S., 2013, Deformation of Central Anatolia: GPS implications: Journal of Geodynamics, v. 67, p. 78–96, https://doi.org/10.1016/j.jog.2012.05.008.

Aydar, E., and Gourgaud, A., 1998, The geology of Mount Hasan stratovolcano, central Anatolia, Turkey: Journal of Volcanology and Geothermal Research, v. 85, p. 129–152, https://doi.org/10.1016/S0377-0273(98)00053-5.

Aydar, E., Schmitt, A.K., Çubukçu, H.E., Akin, L., Ersoy, O., Şen, E., Duncan, R.A., and Atici, G., 2012, Correlation of ignimbrites in the central Anatolian volcanic province using zircon and plagioclase ages and zircon compositions: Journal of Volcanology and Geothermal Research, v. 213, p. 83–97, https://doi.org/10.1016/j.jvolgeores.2011.11.005.

Aydar, E., Çubukçu, H.E., Şen, E., and Akin, L., 2013, Central Anatolian Plateau, Turkey: Incision and paleoaltimetry recorded from volcanic rocks: Turkish Journal of Earth Sciences, v. 22, p. 739–746, https://doi.org/10.3906/yer-1211-8.

Ayhan, M.E., Aktug, B., Acikgoz, M., Ocak, M., Demir, C., Lenk, O., and Reilinger, R.E., 2003, Contemporary crustal deformation in Turkey constrained by global positioning system measurements between 1992 and 2002: Abstract 8781 presented at European Geophysical Society–American Geophysical Union–European Union of Geosciences Joint Assembly, Nice, France, 6–11 April.

Downloaded from https://pubs.geoscienceworld.org/gsa/geosphere/article-pdf/doi/10.1130/GES02175.1/5097193/ges02175.pdf
by guest

Bartol, J., and Govers, R., 2014, A single cause for uplift of the Central and Eastern Anatolian plateau?: Tectonophysics, v. 637, p. 116–136, https://doi.org/10.1016/j.tecto.2014.10.002.
Beker, K., 2002, Biostratigraphic and chronostratigraphic investigation of Ostracoda assemblage of Insuyu limestone (Karapinar/Konya) [M.S. thesis]: Ankara, Turkey, Hacettepe University, 93 p. (in Turkish with English abstract).
Blum, M.D., and Törnqvist, T.E., 2000, Fluvial responses to climate and sea-level change: A review and look forward: Sedimentology, v. 47, p. 2–48, https://doi.org/10.1046/j.1365-3091.2000.00008.x.
Bookhagen, B., and Strecker, M.R., 2012, Spatiotemporal trends in erosion rates across a pronounced rainfall gradient: Examples from the southern Central Andes: Earth and Planetary Science Letters, v. 327, p. 97–110, https://doi.org/10.1016/j.epsl.2012.02.005.
Brown, M., 1994, The generation, segregation, ascent and emplacement of granite magma: The migmatite-to-crustally-derived granite connection in thickened orogens: Earth-Science Reviews, v. 36, p. 83–130, https://doi.org/10.1016/0012-8252(94)90009-4.
Bull, J.M., Minshull, T.A., Mitchell, N.C., Thors, K., Dix, J.K., and Best, A.I., 2003, Fault and magmatic interaction within Iceland's western rift over the last 9 kyr: Geophysical Journal International, v. 154, p. F1–F8, https://doi.org/10.1046/j.1365-246X.2003.01990.x.
Bull, W.B., and McFadden, L.D., 1977, Tectonic geomorphology north and south of the Garlock fault, California, *in* Geomorphology in Arid Regions: Proceedings of the 8th Annual Geomorphology Symposium, p. 115–137.
Çemen, İ., Göncüoglu, M.C., and Dirik, K., 1999, Structural evolution of the Tuzgölü basin in Central Anatolia, Turkey: The Journal of Geology, v. 107, p. 693–706, https://doi.org/10.1086/314379.
Clark, M.K., House, M.A., Royden, L.H., Whipple, K.X., Burchfiel, B.C., Zhang, X., and Tang, W., 2005, Late Cenozoic uplift of southeastern Tibet: Geology, v. 33, p. 525–528, https://doi.org/10.1130/G21265.1.
Ćorić, S., Harzhauser, M., Rögl, F., İslamoğlu, Y., and Landau, B., 2012, Biostratigraphy of some mollusk-bearing middle Miocene localities on the Karaman high plain (Turkey, Konya province): Cainozoic Research, v. 9, no. 2, p. 281–288.
Cosentino, D., Schildgen, T.F., Cipollari, P., Faranda, C., Gliozzi, E., Hudáčková, N., and Strecker, M.R., 2012, Late Miocene surface uplift of the southern margin of the Central Anatolian Plateau, Central Taurides, Turkey: Geological Society of America Bulletin, v. 124, p. 133–145, https://doi.org/10.1130/B30466.1.
Cyr, A.J., Granger, D.E., Olivetti, V., and Molin, P., 2010, Quantifying rock uplift rates using channel steepness and cosmogenic nuclide–determined erosion rates: Examples from northern and southern Italy: Lithosphere, v. 2, p. 188–198, https://doi.org/10.1130/L96.1.
Cyr, A.J., Granger, D.E., Olivetti, V., and Molin, P., 2014, Distinguishing between tectonic and lithologic controls on bedrock channel longitudinal profiles using cosmogenic ^{10}Be erosion rates and channel steepness index: Geomorphology, v. 209, p. 27–38, https://doi.org/10.1016/j.geomorph.2013.12.010.
Davies, J.H., and von Blanckenburg, F., 1995, Slab breakoff: A model of lithosphere detachment and its test in the magmatism and deformation of collisional orogens: Earth and Planetary Science Letters, v. 129, p. 85–102, https://doi.org/10.1016/0012-821X(94)00237-S.
Dawers, N.H., Anders, M.H., and Scholz, C.H., 1993, Growth of normal faults: Displacement-length scaling: Geology, v. 21, p. 1107–1110, https://doi.org/10.1130/0091-7613(1993)021<1107:GONFDL>2.3.CO;2.
Delph, J.R., Biryol, C.B., Beck, S.L., Zandt, G., and Ward, K.M., 2015, Shear wave velocity structure of the Anatolian Plateau: Anomalously slow crust in southwestern Turkey: Geophysical Journal International, v. 202, p. 261–276, https://doi.org/10.1093/gji/ggv141.
Delph, J.R., Abgarmi, B., Ward, K.M., Beck, S.L., Özacar, A.A., Zandt, G., Sandvol, E., Türkelli, N., and Kalafat, D., 2017, The effects of subduction termination on the continental lithosphere: Linking volcanism, deformation, surface uplift, and slab tearing in central Anatolia: Geosphere, v. 13, p. 1788–1805, https://doi.org/10.1130/GES01478.1.
Deniel, C., Aydar, E., and Gourgaud, A., 1998, The Hasan Dagi stratovolcano (Central Anatolia, Turkey): Evolution from calc-alkaline to alkaline magmatism in a collision zone: Journal of Volcanology and Geothermal Research, v. 87, p. 275–302, https://doi.org/10.1016/S0377-0273(98)00097-3.
Densmore, A.L., Dawers, N.H., Gupta, S., Guidon, R., and Goldin, T., 2004, Footwall topographic development during continental extension: Journal of Geophysical Research, v. 109, F03001, https://doi.org/10.1029/2003JF000115.
Densmore, A.L., Dawers, N.H., Gupta, S., and Guidon, R., 2005, What sets topographic relief in extensional footwalls?: Geology, v. 33, p. 453–456, https://doi.org/10.1130/G21440.1.
Dercourt, J., Ricou, L.E., and Vrielynck, B., eds., 1993, Atlas Tethys palaeoenvironmental maps: Paris, Commission pour le Carte Géologique du Monde, 22 plates, 307 p.
Derman, S., Rojay, B., Güney, H., and Yıldız, M., 2003, New sedimentological data on the evolution of Şereflikoçhisar-Aksaray fault zone: Turkish Association of Petroleum Geologists Special Publication 5, p. 47–70 (in Turkish with English abstract).
Dewey, J.F., and Şengör, A.M.C., 1979, Aegean and surrounding regions: Complex multiplate and continuum tectonics in a convergent zone: Geological Society of America Bulletin, v. 90, p. 84–92, https://doi.org/10.1130/0016-7606(1979)90<84:AASRCM>2.0.CO;2.
Dewey, J.F., Hempton, M.R., Kidd, W.S.F., Saroglu, F.T., and Şengör, A.M.C., 1986, Shortening of continental lithosphere: The neotectonics of Eastern Anatolia—A young collision zone, *in* Coward, M.P., and Ries, A.C., eds., Collision Tectonics: Geological Society of London Special Publication 19, p. 1–36, https://doi.org/10.1144/GSL.SP.1986.019.01.01.
Dhont, D., Chorowicz, J., Yürür, T., Froger, J.-L., Köse, O., and Gündogdu, N., 1998, Emplacement of volcanic vents and geodynamics of Central Anatolia, Turkey: Journal of Volcanology and Geothermal Research, v. 85, p. 33–54, https://doi.org/10.1016/S0377-0273(98)00048-1.
Dönmez, M., and Akçay, A.E., 2005, Geologic map of the Aksaray—L31 quadrangle: Ankara, General Directorate of Mineral Research and Exploration of Turkey, scale 1:100,000.
Dönmez, M., Akçay, A.E., Kara, H., Türkecan, A., Yergök, A.F., and Esentürk, K., 2005, Geologic map of the Aksaray—L32 quadrangle: Ankara, General Directorate of Mineral Research and Exploration of Turkey, scale 1:100,000.
Duretz, T., Gerya, T.V., and May, D.A., 2011, Numerical modelling of spontaneous slab breakoff and subsequent topographic response: Tectonophysics, v. 502, no. 1, p. 244–256, https://doi.org/10.1016/j.tecto.2010.05.024.
Duvall, A., Kirby, E., and Burbank, D., 2004, Tectonic and lithologic controls on bedrock channel profiles and processes in coastal California: Journal of Geophysical Research, v. 109, F03002, https://doi.org/10.1029/2003JF000086.
Ekström, G., Nettles, M., and Dziewoński, A.M., 2012, The global CMT project 2004–2010: Centroid-moment tensors for 13,017 earthquakes: Physics of the Earth and Planetary Interiors, v. 200, p. 1–9, https://doi.org/10.1016/j.pepi.2012.04.002.
Emre, Ö., Duman, T.Y., Özalp, S., Şaroğlu, F., Olgun, Ş., Elmacı, H., and Çan, T., 2018, Active fault database of Turkey: Bulletin of Earthquake Engineering, v. 16, p. 3229–3275, https://doi.org/10.1007/s10518-016-0041-2.
Faccenna, C., and Becker, T.W., 2010, Shaping mobile belts by small-scale convection: Nature, v. 465, p. 602–605, https://doi.org/10.1038/nature09064.
Fernández-Blanco, D., 2014, Evolution of orogenic plateaus at subduction margins: Sinking and raising the southern margin of the Central Anatolian Plateau [Ph.D. thesis]: Amsterdam, Vrije Universiteit Amsterdam, 226 p.
Fernández-Blanco, D., Bertotti, G., and Çiner, T.A., 2013, Cenozoic tectonics of the Tuz Gölü Basin (Central Anatolian Plateau, Turkey): Turkish Journal of Earth Sciences, v. 22, p. 715–738, https://doi.org/10.3906/yer-1206-7.
Fernández-Blanco, D., Bertotti, G., Aksu, A., and Hall, J., 2018, Monoclinal flexure of an orogenic plateau margin during subduction, south Turkey: Basin Research, v. 31, p. 709–727, https://doi.org/10.1111/bre.12341.
Genç, Y., and Yürür, M.T., 2010, Coeval extension and compression in Late Mesozoic–Recent thin-skinned extensional tectonics in central Anatolia, Turkey: Journal of Structural Geology, v. 32, p. 623–640, https://doi.org/10.1016/j.jsg.2010.03.011.
Geological Research Department, 1989a, Geological map of the Aksaray—H17 quadrangle: Ankara, General Directorate of Mineral Research and Exploration of Turkey, scale 1:100,000.
Geological Research Department, 1989b, Geologic map of the Aksaray—H18 quadrangle: Ankara, General Directorate of Mineral Research and Exploration of Turkey, scale 1:100,000.
Geological Research Department, 1990, Geologic map of the Kırşehir—G17 quadrangle: Ankara, General Directorate of Mineral Research and Exploration of Turkey, scale 1:100,000.
Göğüş, O.H., Pysklywec, R.N., Şengör, A.M.C., and Gün, E., 2017, Drip tectonics and the enigmatic uplift of the Central Anatolian Plateau: Nature Communications, v. 8, 1538, https://doi.org/10.1038/s41467-017-01611-3.
Görür, N., and Derman, A.S., 1978, Tuz Golu-Haymana havzasinin stratigrafik ve tektonik analizi: Ankara, Turkish Petroleum Corporation (TPAO) Report 1514.
Görür, N., Oktay, F.Y., Seymen, İ., and Şengör, A.M.C., 1984, Palaeotectonic evolution of the Tuzgölü basin complex, Central Turkey: Sedimentary record of a Neo-Tethyan closure, *in* Dixon, J.E. and Robertson, A.H.F, eds., The Geological Evolution of the Eastern Mediterranean: Geological Society of London Special Publication 17, p. 467–482, https://doi.org/10.1144/GSL.SP.1984.017.01.34.

Downloaded from https://pubs.geoscienceworld.org/gsa/geosphere/article-pdf/doi/10.1130/GES02175.1/5097193/ges02175.pdf
by guest

Gürbüz, A., and Kazancı, N., 2014, Facies characteristics and control mechanisms of Quaternary deposits in the Tuz Gölü basin: Bulletin of the Mineral Research and Exploration, v. 149, p. 1–18, https://doi.org/10.19111/bmre.63616.

Gutscher, M.-A., Spakman, W., Bijwaard, H., and Engdahl, E.R., 2000, Geodynamics of flat subduction: Seismicity and tomographic constraints from the Andean margin: Tectonics, v. 19, p. 814–833, https://doi.org/10.1029/1999TC001152.

Hack, J.T., 1957, Studies of longitudinal stream profiles in Virginia and Maryland: U.S. Geological Survey Professional Paper 294-B, p. 45–97, https://doi.org/10.3133/pp294B.

Hancock, G., and Willgoose, G., 2001, Use of a landscape simulator in the validation of the SIBERIA catchment evolution model: Declining equilibrium landforms: Water Resources Research, v. 37, p. 1981–1992, https://doi.org/10.1029/2001WR900002.

Hare, P.W., and Gardner, T.W., 1985, Geomorphic indicators of vertical neotectonism along converging plate margins, Nicoya Peninsula, Costa Rica, *in* Morisawa, M., and Hack, J.T., eds., Tectonic Geomorphology: Proceedings of the 15th Annual Binghamton Geomorphology Symposium: Boston, Massachusetts, Allen and Unwin, p. 75–104.

Higgins, M., Schoenbohm, L.M., Brocard, G., Kaymakcı, N., Gosse, J.C., and Cosca, M.A., 2015, New kinematic and geochronologic evidence for the Quaternary evolution of the Central Anatolian fault zone (CAFZ): Tectonics, v. 34, p. 2118–2141, https://doi.org/10.1002/2015TC003864.

Jackson, J., and Molnar, P., 1990, Active faulting and block rotations in the western Transverse Ranges, California: Journal of Geophysical Research, v. 95, p. 22,073–22,087, https://doi.org/10.1029/JB095iB13p22073.

Jolivet, L., Faccenna, C., Huet, B., Labrousse, L., Le Pourhiet, L., Lacombe, O., Lecomte, E., Burov, E., Denèle, Y., Brun, J.-P., Philippon, M., Paul, A., Salaün, G., Karabulut, H., Piromallo, C., Monié, P., Gueydan, F., Okay, A.I., Oberhänsli, R., Pourteau, A., Augier, R., Gadenne, L., and Driussi, O., 2013, Aegean tectonics: Strain localisation, slab tearing and trench retreat: Tectonophysics, v. 597–598, p. 1–33, https://doi.org/10.1016/j.tecto.2012.06.011.

Jones, C.H., Farmer, G.L., and Unruh, J., 2004, Tectonics of Pliocene removal of lithosphere of the Sierra Nevada, California: Geological Society of America Bulletin, v. 116, p. 1408–1422, https://doi.org/10.1130/B25397.1.

Jordan, T.E., Isacks, B.L., Allmendinger, R.W., Brewer, J.A., Ramos, V.A., and Ando, C.J., 1983, Andean tectonics related to geometry of subducted Nazca plate: Geological Society of America Bulletin, v. 94, p. 341–361, https://doi.org/10.1130/0016-7606(1983)94<341:ATRTGO>2.0.CO;2.

JPL (Jet Propulsion Laboratory), 2004, ASTER: https://asterweb.jpl.nasa.gov/gdem.asp (version 1 last accessed October 2012).

Kay, R.W., and Mahlburg Kay, S., 1993, Delamination and delamination magmatism: Tectonophysics, v. 219, p. 177–189, https://doi.org/10.1016/0040-1951(93)90295-U.

Kay, S.M., Coira, B., and Viramonte, J., 1994, Young mafic back arc volcanic rocks as indicators of continental lithospheric delamination beneath the Argentine Puna Plateau, central Andes: Journal of Geophysical Research, v. 99, p. 24,323–24,339, https://doi.org/10.1029/94JB00896.

Kaymakcı, N., Inceöz, M., and Ertepinar, P., 2006, 3D-architecture and Neogene evolution of the Malayta Basin: Inferences for the kinematics of the Malatya and Ovacık fault zones: Turkish Journal of Earth Sciences, v. 15, p. 123–154.

Keller, E.A., and Pinter, N., 2002, Active Tectonics: Earthquakes, Uplift and Landscape: Upper Saddle River, New Jersey, Prentice-Hall Inc., 362 p.

Kent, E., Boulton, S.J., Whittaker, A.C., Stewart, I.S., and Alçiçek, M.C., 2017, Normal fault growth and linkage in the Gediz (Alaşehir) Graben, Western Turkey, revealed by transient river long-profiles and slope-break knickpoints: Earth Surface Processes and Landforms, v. 42, p. 836–853, https://doi.org/10.1002/esp.4049.

Ketin, I., 1948, Über die tektonisch-mechanischen Folgerungen aud den grossen anatolischen Erdbeben des letzten Dezenniums: Geologische Rundschau, v. 36, p. 77–83, https://doi.org/10.1007/BF01791916.

Kim, Y.-S., and Sanderson, D.J., 2005, The relationship between displacement and length of faults: A review: Earth-Science Reviews, v. 68, p. 317–334, https://doi.org/10.1016/j.earscirev.2004.06.003.

Kirby, E., and Whipple, K.X., 2012, Expression of active tectonics in erosional landscapes: Journal of Structural Geology, v. 44, p. 54–75, https://doi.org/10.1016/j.jsg.2012.07.009.

Kirby, E., Whipple, K.X., Tang, W., and Chen, Z., 2003, Distribution of active rock uplift along the eastern margin of the Tibetan Plateau: Inferences from bedrock channel longitudinal profiles: Journal of Geophysical Research, v. 108, 2217, https://doi.org/10.1029/2001JB000861.

Koç, A., and Kaymakcı, N., 2013, Kinematics of the Sürgü Fault Zone (Malatya, Turkey): A remote sensing study: Journal of Geodynamics, v. 65, p. 292–307, https://doi.org/10.1016/j.jog.2012.08.001.

Koçyiğit, A., and Beyhan, A., 1998, A new intracontinental transcurrent structure: The Central Anatolian Fault Zone, Turkey: Tectonophysics, v. 284, p. 317–336, https://doi.org/10.1016/S0040-1951(97)00176-5.

Koçyiğit, A., and Özacar, A.A., 2003, Extensional neotectonic regime through the NE edge of the outer Isparta Angle, SW Turkey: New field and seismic data: Turkish Journal of Earth Sciences, v. 12, p. 67–90.

Kürçer, A., and Gökten, Y.E., 2012, Paleoseismological three dimensional virtual photography method—A case study: Bağlarkayası-2010 trench, Tuz Gölü Fault Zone, Central Anatolia, Turkey, *in* Sharkov, E., ed., Tectonics—Recent Advances: IntechOpen, https://doi.org/10.5772/48194.

Landau, B.M., Harzhauser, M., İslamoğlu, Y., and Marques de Silva, C., 2013, Systematics and paleobiogeography of the gastropods of the middle Miocene (Serravallian) Karaman Basin, Turkey: Cainozoic Research, v. 11–13, p. 3–584.

Langbein, W.B., 1947, Topographic characteristics of drainage basins: U.S. Geological Survey Water-Supply Paper 968-C, p. 125–157, https://doi.org/10.3133/wsp968C.

Le Pichon, X., 1982, Land-locked oceanic basins and continental collision: The Eastern Mediterranean as a case example, *in* Hsü, K., ed., Mountain Building Processes: London, Academic Press, p. 201–211.

Lepetit, P., Viereck, L., Piper, J.D.A., Sudo, M., Gürel, A., Çopuroğlu, I., Gruber, M., Mayer, B., Koch, M., Tatar, O., and Gürsoy, H., 2014, $^{40}Ar/^{39}Ar$ dating of ignimbrites and plinian air-fall layers from Cappadocia, Central Turkey: Implications to chronostratigraphic and Eastern Mediterranean palaeoenvironmental record: Geochemistry, v. 74, p. 471–488, https://doi.org/10.1016/j.chemer.2014.05.001.

Mathieu, L., van Wyk de Vries, B., Pilato, M., and Troll, V.R., 2011, The interaction between volcanoes and strike-slip, transtensional, and transpressional fault zones: Analogue models and natural examples: Journal of Structural Geology, v. 33, p. 898–906, https://doi.org/10.1016/j.jsg.2011.03.003.

McClusky, S., Balassanian, S., Barka, A., Demir, C., Ergintav, S., Georgiev, I., Gurkan, O., Hamburger, M., Hurst, K., Kahle, H., Kastens, K., Kekelidze, G., King, R., Kotzev, V., Lenk, O., Mahmoud, S., Mishin, A., Nadariya, M., Ouzonis, A., Paradissis, D., Peter Y., Prilepin, M., Reilinger, R., Sanli, I., Seeger, H., Tealeb, A., Toksöz, M.N., and Veis, G., 2000, Global Positioning System constraints on plate kinematics and dynamics in the eastern Mediterranean and Caucasus: Journal of Geophysical Research, v. 105, p. 5695–5720, https://doi.org/10.1029/1999JB900351.

McKenzie, D., 1972, Active tectonics of the Mediterranean region: Geophysical Journal International, v. 30, p. 109–185, https://doi.org/10.1111/j.1365-246X.1972.tb02351.x.

McKenzie, D., 1976, The East Anatolian Fault: A major structure in eastern Turkey: Earth and Planetary Science Letters, v. 29, p. 189–193, https://doi.org/10.1016/0012-821X(76)90038-8.

Meijers, M.J.M., Brocard, G.Y., Cosca, M.A., Ludecke, T., Teyssier, C., Whitney, D.L., and Mulch, A., 2018, Rapid late Miocene surface uplift of the Central Anatolian Plateau margin: Earth and Planetary Science Letters, v. 497, p. 29–41, https://doi.org/10.1016/j.epsl.2018.05.040.

Meijers, M.J.M., Brocard, G.Y., Whitney, D.L., and Mulch, A., 2019, Paleoenvironmental conditions and drainage evolution of the central Anatolian lake system (Turkey) during late Miocene to Pliocene surface uplift: Geosphere, v. 16, p. 490–509, https://doi.org/10.1130/GES02135.1.

Melnick, D., Yıldırım, C., Hillemann, C., Garcin, Y., Çiner, A., Pérez-Gussinyé, M., and Strecker, M.R., 2017, Slip along the Sultanhanı Fault in Central Anatolia from deformed Pleistocene shorelines of palaeo-lake Konya and implications for seismic hazards in low-strain regions: Geophysical Journal International, v. 209, p. 1431–1454, https://doi.org/10.1093/gji/ggx074.

Niemann, J.D., Gasparini, N.M., Tucker, G.E., and Bras, R.L., 2001, A quantitative evaluation of Playfair's law and its use in testing long-term stream erosion models: Earth Surface Processes and Landforms, v. 26, p. 1317–1332, https://doi.org/10.1002/esp.272.

Notsu, K., Fujitani, T., Ui, T., Matsuda, J., and Ercan, T., 1995, Geochemical features of collision-related volcanic rocks in central and eastern Anatolia, Turkey: Journal of Volcanology and Geothermal Research, v. 64, p. 171–192, https://doi.org/10.1016/0377-0273(94)00077-T.

Özkaymak, C., and Sözbilir, H., 2012, Tectonic geomorphology of the Spildağı High Ranges, western Anatolia: Geomorphology, v. 173–174, p. 128–140, https://doi.org/10.1016/j.geomorph.2012.06.003.

Özsayın, E., and Dirik, K., 2011, The role of oroclinal bending in the structural evolution of the Central Anatolian Plateau: Evidence of a regional changeover from shortening to extension: Geologica Carpathica, v. 62, p. 345–359, https://doi.org/10.2478/v10096-011-0026-7.

Özsayın, E., Çiner, T.A., Rojay, F.B., Dirik, R.K., Melnick, D., Fernández-Blanco, D., Bertotti, G., Schildgen, T.F., Garcin, Y., Strecker, M.R., and Sudo, M., 2013, Plio-Quaternary extensional tectonics of the Central Anatolian Plateau: A case study from the Tuz Gölü Basin, Turkey: Turkish Journal of Earth Sciences, v. 22, p. 691–714, https://doi.org/10.3906/yer-1210-5.

Downloaded from https://pubs.geoscienceworld.org/gsa/geosphere/article-pdf/doi/10.1130/GES02175.1/5097193/ges02175.pdf
by guest

Paulsen, T.S., and Wilson, T.J., 2010, New criteria for systematic mapping and reliability assessment of monogenetic volcanic vent alignments and elongate volcanic vents for crustal stress analyses: Tectonophysics, v. 482, p. 16–28, https://doi.org/10.1016/j.tecto.2009.08.025.

Pike, R.J., and Wilson, S.E., 1971, Elevation-relief ratio, hypsometric integral, and geomorphic area-altitude analysis: Geological Society of America Bulletin, v. 82, p. 1079–1084, https://doi.org/10.1130/0016-7606(1971)82[1079:ERHIAG]2.0.CO;2.

Platzman, E.S., Tapirdamaz, C., and Sanver, M., 1998, Neogene anticlockwise rotation of central Anatolia (Turkey): Preliminary palaeomagnetic and geochronological results: Tectonophysics, v. 299, p. 175–189, https://doi.org/10.1016/S0040-1951(98)00204-2.

Popov, S.V., Rögl, F., Rozanov, A.Y., Steiniger, F.F., Shcherba, I.G., and Kovac, M., 2004, Lithological-paleogeographic maps of Paratethys: 10 maps late Eocene to Pliocene: Courier Forschungsinstitut Senckenberg, v. 250, 73 p.

Popov, S.V., Shcherba, I.G., Ilyina, L.B., Nevesskaya, L.A., Paramonova, N.P., Khondkarian, S.O., and Magyar, I., 2006, Late Miocene to Pliocene palaeogeography of the Paratethys and its relation to the Mediterranean: Palaeogeography, Palaeoclimatology, Palaeoecology, v. 238, p. 91–106, https://doi.org/10.1016/j.palaeo.2006.03.020.

Price, S.P., and Scott, B., 1994, Fault-block rotations at the edge of a zone of continental extension, southwest Turkey: Journal of Structural Geology, v. 16, p. 381–392, https://doi.org/10.1016/0191-8141(94)90042-6.

Reid, M.R., Schleiffarth, W.K., Cosca, M.A., Delph, J.R., Blichert-Toft, J., and Cooper, K.M., 2017, Shallow melting of MORB-like mantle under hot continental lithosphere, Central Anatolia: Geochemistry Geophysics Geosystems, v. 18, p. 1866–1888, https://doi.org/10.1002/2016GC006772.

Reilinger, R., McClusky, S., Vernant, P., Lawrence, S., Ergintav, S., Cakmak, R., Ozener, H., Kadirov, F., Guliuv, I., Stepanyan, R., Nadariya, M., Hahubia, G., Mahmoud, S., Sakr, K., ArRajehi, A., Paradissis, D., Al-Aydrus, A., Prilepin, M., Guseva, T., Evren, E., Dmitrotsa, A., Filikov, S.V., Gomez, F., Al-Ghazzi, R., and Karam, G., 2006, GPS constraints on continental deformation in the Africa-Arabia-Eurasia continental collision zone and implications for the dynamics of plate interactions: Journal of Geophysical Research, v. 111, B05411, https://doi.org/10.1029/2005JB004051.

Reilinger, R.E., McClusky, S.C., Oral, M.B., King, R.W., Toksoz, M.N., Barka, A.A., Kinik, I., Lenk, O., and Sanli, I., 1997, Global Positioning System measurements of present-day crustal movements in the Arabia-Africa-Eurasia plate collision zone: Journal of Geophysical Research, v. 102, p. 9983–9999, https://doi.org/10.1029/96JB03736.

Robertson, A.H.F., Dixon, J.E., Brown, S., Collins, A., Morris, A., Pickett, E., Sharp, I., and Ustaömer, T., 1996, Alternative tectonic models for the Late Palaeozoic–Early Tertiary development of Tethys in the Eastern Mediterranean region, *in* Morris, A., and Tarling, D.H., eds, Palaeomagnetism and Tectonics of the Mediterranean Region: Geological Society of London Special Publication 105, p. 239–263, https://doi.org/10.1144/GSL.SP.1996.105.01.22.

Robertson, A.H.F., Parlak, O., and Ustaömer, T., 2009, Melange genesis and ophiolite emplacement related to subduction of the northern margin of the Tauride-Anatolide continent, central and western Turkey, *in* Van Hinsbergen, D.J.J., Edwards, M.A., and Govers, R., eds., Collision and Collapse at the Africa-Arabia-Eurasia Subduction Zone: Geological Society of London Special Publication 311, p. 9–66, https://doi.org/10.1144/SP311.2.

Robl, J., Heberer, B., Prasicek, G., Neubauer, F., and Hergarten, S., 2017, The topography of a continental indenter: The interplay between crustal deformation, erosion, and base level changes in the eastern Southern Alps: Journal of Geophysical Research: Earth Surface, v. 122, p. 310–334, https://doi.org/10.1002/2016JF003884.

Rockwell, T.K., Keller, E.A., and Johnson, D.L., 1985, Tectonic geomorphology of alluvial fans and mountain fronts near Ventura, California, *in* Morisawa, M., and Hack, J.T., eds, Tectonic Geomorphology: Proceedings of the 15th Annual Binghamton Geomorphology Symposium: Boston, Massachusetts, Allen and Unwin, p. 183–207.

Rosenbloom, N.A., and Anderson, R.S., 1994, Hillslope and channel evolution in a marine terraced landscape, Santa Cruz, California: Journal of Geophysical Research, v. 99, p. 14,013–14,029, https://doi.org/10.1029/94JB00048.

Schattner, U., 2010, What triggered the early-to-mid Pleistocene tectonic transition across the entire eastern Mediterranean?: Earth and Planetary Science Letters, v. 289, p. 539–548, https://doi.org/10.1016/j.epsl.2009.11.048.

Schildgen, T.F., Cosentino, D., Bookhagen, B., Niedermann, S., Yıldırım, C., Echtler, H.P., and Strecker, M.R., 2012a, Multi-phased uplift of the southern margin of the Central Anatolian plateau, Turkey: A record of tectonic and upper mantle processes: Earth and Planetary Science Letters, v. 317, p. 85–95, https://doi.org/10.1016/j.epsl.2011.12.003.

Schildgen, T.F., Cosentino, D., Caruso, A., Buchwaldt, R., Yıldırım, C., Bowring, S.A., Rojay, B., Echtler, H., and Strecker, M.R., 2012b, Surface expression of eastern Mediterranean slab dynamics: Neogene topographic and structural evolution of the southwest margin of the Central Anatolian Plateau, Turkey: Tectonics, v. 31, TC2005, https://doi.org/10.1029/2011TC003021.

Schildgen, T.F., Yıldırım, C., Cosentino, D., and Strecker, M.R., 2014, Linking slab break-off, Hellenic trench retreat, and uplift of the Central and Eastern Anatolian plateaus: Earth-Science Reviews, v. 128, p. 147–168, https://doi.org/10.1016/j.earscirev.2013.11.006.

Schlieffarth, W.K., Darin, M.H., Reid, M.R., and Umhoefer, P.J., 2019, Dynamics of episodic late Cretaceous-Cenozoic magmatism across Central to Eastern Anatolia: New insights from an extensive geochronology compilation: Geosphere, v. 14, p. 1990–2008, https://doi.org/10.1130/GES01647.1.

Schoenbohm, L.M., Whipple, K.X., Burchfiel, B.C., and Chen, L., 2004, Geomorphic constraints on surface uplift, exhumation, and plateau growth in the Red River region, Yunnan Province, China: Geological Society of America Bulletin, v. 116, p. 895–909, https://doi.org/10.1130/B25364.1.

Schumm, S.A., 1956, Evolution of drainage systems and slopes in badlands at Perth Amboy, New Jersey: Geological Society of America Bulletin, v. 67, p. 597–646, https://doi.org/10.1130/0016-7606(1956)67[597:EODSAS]2.0.CO;2.

Şen, P.A., Temel, A., and Gourgaud, A., 2004, Petrogenetic modeling of Quaternary post-collisional volcanism: A case study of Entral and Eastern Anatolia: Geological Magazine, v. 141(1), p. 81–98, https://doi.org/10.1017/S001675683008550.

Şengör, A.M.C., and Kidd, W.S.F., 1979, Post-collisional tectonics of the Turkish-Iranian plateau and a comparison with Tibet: Tectonophysics, v. 55, p. 361–376, https://doi.org/10.1016/0040-1951(79)90184-7.

Şengör, A.M.C., and Yılmaz, Y., 1981, Tethyan evolution of Turkey: A plate tectonic approach: Tectonophysics, v. 75, p. 181–241, https://doi.org/10.1016/0040-1951(81)90275-4.

Şengör, A.M.C., Görür, N., and Şaroğlu, F., 1985, Strike-slip faulting and related basin formation in zones of tectonic escape: Turkey as a case study, *in* Biddle, K.T., and Christie-Blick, N., eds., Strike-Slip Faulting, Basin Formation, and Sedimentation: Society of Economic Paleontologists and Mineralogists Special Publication 37, p. 227–264, https://doi.org/10.2110/pec.85.37.0227.

Simão, N.M., Nalbant, S.S., Sunbul, F., and Komec Mutlu, A., 2016, Central and eastern Anatolian crustal deformation rate and velocity fields derived from GPS and earthquake data: Earth and Planetary Science Letters, v. 422, p. 89–98, doi:10.1016/j.epsl.2015.10.041.

Small, E.E., and Anderson, R.S., 1998, Pleistocene relief production in Laramide mountain ranges, western United States: Geology, v. 26, p. 123–126, https://doi.org/10.1130/0091-7613(1998)026<0123:PRPILM>2.3.CO;2.

Sólyom, P.B., and Tucker, G.E., 2007, The importance of the catchment area-length relationship in governing non-steady state hydrology, optimal junction angles and drainage network patters: Geomorphology, v. 88, p. 84–108, doi:10.1016/j.geomorph.2006.10.014.

Strahler, A.N., 1952, Hypsometric (area-altitude) analysis of erosional topography: Geological Society of America Bulletin, v. 63, p. 1117–1142, https://doi.org/10.1130/0016-7606(1952)63[1117:HAAOET]2.0.CO;2.

Suresh, R., 2000, Soil and Water Conservation Engineering (third edition): Delhi, Standard Publishers, p. 785–813.

Tatar, O., Piper, J.D.A., Gürsoy, H., and Temiz, H., 1996, Regional significance of neotectonic counterclockwise rotation in central Turkey: International Geology Review, v. 38, p. 692–700, https://doi.org/10.1080/00206819709465353.

Toprak, V., 1998, Vent distribution and its relation to regional tectonics, Cappadocian Volcanics, Turkey: Journal of Volcanology and Geothermal Research, v. 85, p. 55–67, https://doi.org/10.1016/S0377-0273(98)00049-3.

Umhoefer, P.J., Whitney, D.L., Teyssier, C., Fayon, A.K., Casale, G., and Heizler, M.T., 2007, Yo-yo tectonics in a wrench zone, Central Anatolian fault zone, Turkey, *in* Roeske, S.M., Till, A.B., Foster, D.A., and Sample, J.C., eds., Exhumation Associated with Continental Strike-Slip Fault Systems: Geological Society of America Special Paper 434, p. 35–57, https://doi.org/10.1130/2007.2434(03).

U.S. Geological Survey, 2019, HydroSHEDS: http://hydrosheds.cr.usgs.gov/index.php (last accessed October 2012).

Villamor, P., Van Dissen, R., Alloway, B.V., Palmer, A.S., and Litchfield, N., 2007, The Rangipo fault, Taupo rift, New Zealand: An example of temporal slip-rate and single-event displacement variability in a volcanic environment: Geological Society of America Bulletin, v. 119, p. 529–547, https://doi.org/10.1130/B26000.1.

Downloaded from https://pubs.geoscienceworld.org/gsa/geosphere/article-pdf/doi/10.1130/GES02175.1/5097193/ges02175.pdf
by guest

Walsh, L.S., Martin, A.J., Ojha, T.P., and Fedenczuk, T., 2012, Correlations of fluvial knickzones with landslide dams, lithologic contacts, and faults in the southwestern Annapurna Range, central Nepalese Himalaya: Journal of Geophysical Research, v. 117, F01012, https://doi.org/10.1029/2011JF001984.

Walsh-Kennedy, S., Aksu, A.E., Hall, J., Hiscott, R.N., Yaltırak, C., and Çilfçi, G., 2014, Source to sink: The development of the latest Messinian to Pliocene–Quaternary Cilicia and Adana Basins and their linkages with the onland Mut Basin, eastern Mediterranean: Tectonophysics, v. 622, p. 1–21, https://doi.org/10.1016/j.tecto.2014.01.019.

Wang, C., Zhao, X., Liu, Z., Lippert, P.C., Graham, S.A., Coe, R.S., Yi, H., Zhu, L., Liu, S., and Li, Y., 2008, Constraints on the early uplift history of the Tibetan Plateau: Proceedings of the National Academy of Sciences of the United States of America, v. 105, p. 4987–4992, https://doi.org/10.1073/pnas.0703595105.

Weissel, J.K., and Seidl, M.A., 1998, Inland propagation of erosional escarpments and river profile evolution across the southeast Australian passive continental margin, *in* Tinkler, K.J., and Wohl, E.E., eds., Rivers Over Rock: Fluvial Processes in Bedrock Channels: American Geophysical Union Geophysical Monograph 107, p. 189–206, https://doi.org/10.1029/GM107p0189.

Westaway, R., 1990, Block rotation in western Turkey: 1. Observational evidence: Journal of Geophysical Research, v. 95, p. 19,857–19,884, https://doi.org/10.1029/JB095iB12p19857.

Westaway, R., Demir, T., and Syrek, A., 2008, Geometry of the Turkey-Arabia and Africa-Arabia plate boundaries in the latest Miocene to mid-Pliocene: The role of the Malatya-Ovacık Fault Zone in eastern Turkey: eEarth, v. 3, p. 27–35, https://doi.org/10.5194/ee-3-27-2008.

Whipple, K.X., and Tucker, G.E., 1999, Dynamics of the stream-power river incision model: Implications for height limits of mountain ranges, landscape response timescales, and research needs: Journal of Geophysical Research, v. 104, p. 17,661–17,674, https://doi.org/10.1029/1999JB900120.

Whipple, K.X., and Tucker, G.E., 2002, Implications of sediment-flux-dependent river incision models for landscape evolution: Journal of Geophysical Research, v. 107, no. B2, https://doi.org/10.1029/2000JB000044.

Whittaker, A.C., and Boulton, S.J., 2012, Tectonic and climatic controls on knickpoint retreat rates and landscape response times: Journal of Geophysical Research, v. 117, F02024, https://doi.org/10.1029/2011JF002157.

Whittaker, A.C., Attal, M., Cowie, P.A., Tucker, G.E., and Roberts, G., 2008, Decoding temporal and spatial patterns of fault uplift using transient river long profiles: Geomorphology, v. 100, p. 506–527, https://doi.org/10.1016/j.geomorph.2008.01.018.

Wobus, C., Whipple, K.X., Kirby, E., Snyder, N., Johnson, J., Spyropolou, K., Crosby, B., and Sheehan, D., 2006, Tectonics from topography: Procedures, promise, and pitfalls, *in* Willet, S.D., Hovius, N., Brandon, M.T., and Fisher, D.M., eds., Tectonics, Climate, and Landscape Evolution: Geological Society of America Special Paper 398, p. 55–74, https://doi.org/10.1130/2006.2398(04).

Yıldırım, C., 2014, Relative tectonic activity assessment of the Tuz Gölü Fault Zone; Central Anatolia, Turkey: Tectonophysics, v. 630, p. 183–192, https://doi.org/10.1016/j.tecto.2014.05.023.

Yildirim, C., Schildgen, T.F., Echtler, H., Melnick, D., and Strecker, M.R., 2011, Late Neogene and active orogenic uplift in the Central Pontides associated with the North Anatolian Fault: Implications for the northern margin of the Central Anatolian Plateau, Turkey: Tectonics, v. 30, TC5005, https://doi.org/10.1029/2010TC002756.

Yılmaz, Y., Tüysüz, O., Yiğitbaş, E., Genç, Ş.C., and Şengör, A.M.C., 1997, Geology and tectonic evolution of the Pontides, *in* Robertson, A.G., ed., Regional and Petroleum Geology of the Black Sea and Surrounding Region: American Association of Petroleum Geologists Memoir 68, p. 183–226, https://doi.org/10.1306/M68612C11.

Yuan, X., Sobolev, S.V., and Kind, R., 2002, Moho topography in the central Andes and its geodynamic implications: Earth and Planetary Science Letters, v. 199, p. 389–402, https://doi.org/10.1016/S0012-821X(02)00589-7.

Zandt, G., Gilbert, H., Owens, T.J., Ducea, M., Saleeby, J., and Jones, C.H., 2004, Active foundering of a continental arc root beneath the southern Sierra Nevada in California: Nature, v. 431, p. 41–46, https://doi.org/10.1038/nature02847.

Downloaded from https://pubs.geoscienceworld.org/gsa/geosphere/article-pdf/doi/10.1130/GES02175.1/5097193/ges02175.pdf
by guest